CHALMERS
UNIVERSITY OF TECHNOLOGY

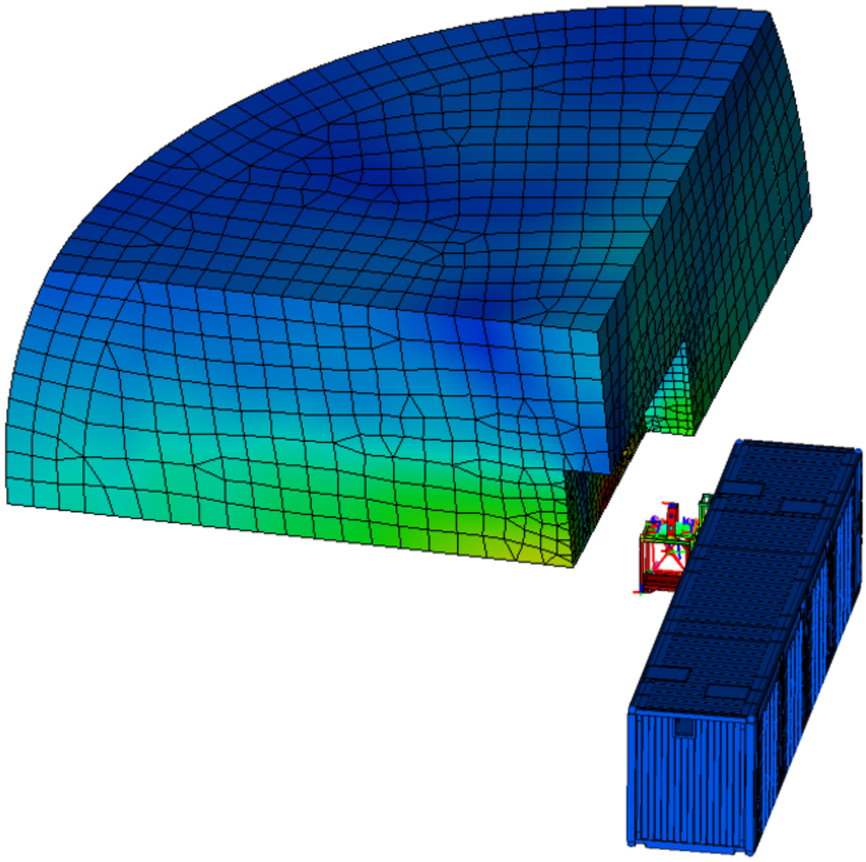

Finite Element Based Method for Investigation of Exterior Acoustics

Stirling Engine Induced Acoustics

Master's thesis in Applied Mechanics

CAROLINE ANSIN
OLIVIA ERIKSSON

Department of Mechanics and Maritime Sciences
CHALMERS UNIVERSITY OF TECHNOLOGY
Gothenburg, Sweden 2020

Master's thesis in Applied Mechanics

Finite Element Based Method for Investigation of Exterior Acoustics

Stirling Engine Induced Acoustics

CAROLINE ANSIN
OLIVIA ERIKSSON

CHALMERS
UNIVERSITY OF TECHNOLOGY

Department of Mechanics and Maritime Sciences
Division of Dynamics
Chalmers University of Technology
Gothenburg, Sweden 2020

Finite Element Based Method for Investigation of Exterior Acoustics
Stirling Engine Induced Acoustics
CAROLINE ANSIN
OLIVIA ERIKSSON

Supervisors: Mats Johansson, Uniso Technologies & Fredrik Karström, Azelio
Examiner: Thomas Abrahamsson, Department of Mechanics and Maritime Sciences

Master’s Thesis 2020:24
Department of Mechanics and Maritime Sciences
Division of Dynamics
Chalmers University of Technology
SE-412 96 Gothenburg
Telephone +46 (0)31 772 1000

Cover image: Displays the exterior sound radiation in a finite element acoustic domain, seen to the left. The domain surrounds a Thermal Energy Storing (TES) System, seen to the right, developed by Azelio. Sound radiates from the system due to vibrations that arise from imbalance loads of the Stirling engine. The Stirling engine is attached to the TES system.

Department of Mechanics and Maritime Sciences
Gothenburg, Sweden 2020

Preface

This report is a master's thesis project regarding the development of a generic numerical method of how to simulate the exterior sound radiation. The project was carried out by two students from the master program Applied Mechanics together with the companies Azelio and Uniso Technologies. The work was done in 20 weeks of the spring semester of 2020 at the Department of Mechanics and Maritime Sciences at Chalmers University of Technology, Sweden.

Through the master's thesis project we have received help from several people that have contributed with knowledge and support. We would like to thank: Our supervisors Mats Johansson and Fredrik Karström for helping us with the field of structural dynamics and acoustics. Our examinor Professor Thomas Abrahamsson for sharing his knowledge when it comes to experimental modal analysis and giving us feedback on the report. Roger Sjöqvist who coordinated the test, where the equipment was borrowed from Chalmers University of Technology. Lastly, Kajsa Bengtsson for helping us with software related issues through our work.

Caroline Ansin
Olivia Eriksson

Gothenburg, June 2020

Finite Element Based Method for Investigation of Exterior Acoustics
Stirling Engine Induced Acoustics
Master's Thesis in Applied Mechanics
CAROLINE ANSIN
OLIVIA ERIKSSON
Department of Mechanics and Maritime Sciences
Division of Dynamics
Chalmers University of Technology

Abstract

A challenge with renewable energy is that the power source is time varying. To be able to supply renewable power at all hours, the company Azelio is developing a Thermal Energy Storing (TES) system. During the development, multiple design changes are made at a rapid pace. Therefore, it is important to utilize numerical tools to save time and money.

Azelio's TES system is Stirling engine based. The free mass loads in the engine causes vibrations, which make sound propagate from the system. The sound level is mostly not an issue since the system will be located in uninhabited areas, but it can be of importance if the system would be serviced during operation. That is why a numerical method for determining the exterior sound level would be of interest. The purpose is, thereby, to develop a generic method that can be used to predict exterior sound. The method will be developed for the current TES system, but should be possible to use when evaluating new designs.

A numerical method for predicting the exterior far field sound level located in a free field was developed using the finite element method in Ansys Mechanical APDL. The exterior acoustics problem was solved using a one-way coupling from structure to fluid. The structural vibrations were computed through mode-superposition in a harmonic analysis, in which the system was assumed to be linear and time-invariant. The vibrations were then used to generate waves in a fluid full harmonic analysis. To validate the numerical model of the system, an experimental modal analysis was performed on the current TES system, but no measurements during operation were made.

Due to the complexity of the system and time restriction, the results from the experiment lacked in correlation with the results from the finite element analysis. However, this does not say anything about the developed sound predicting method. One conclusion that can be drawn is that it is difficult to model and do experiments on a complex system.

The developed method is generic and can be applied to any vibrating system. It can be used to compute the sound pressure level in a plane or a point, at various engine speeds. The sound level in a point can be compared to measurements, while the plane contour plot can be used in the development process to identify parts that radiate a lot of sound. The method was developed for a complex system and should be tested on a simpler system. To validate the method, various tests should be performed.

Keywords: Finite Element Method (FEM), Modal Analysis, Harmonic Analysis, Superposition, Experimental Modal Analysis (EMA), Exterior Acoustics, One-Way Coupling, Far Field, Stirling Engine

Notations

Abbreviations

ABE Absorbing Boundary Element

AML Artifically Matched Layer

APDL Ansys Parametric Design Language

BC Boundary Condition

BEM Boundary Element Method

COG Centre of Gravity

DAQ Data Acquisition

DFT Discrete Fourier Transform

DOF Degree of Freedom

EMA Experimental Modal Analysis

FE Finite Element

FEA Finite Element Analysis

FEM Finite Element Method

FFT Fast Fourier Transform

FRAC Frequency Response Assurance Criterion

FRF Frequency Response Function

FSI Fluid Structural Interaction

IRB Infinite Radiation Boundary

NRMSE Norm of Square Error

PCG Preconditioned Conjugate Gradients

PCS Power Conversion System

SSM State-Space Model

TES Thermal Energy Storage

WBT Wave Based Technique

General notation

$\ddot{x}$ Second time derivative of x

$\dot{x}$ Time derivative of x

$\hat{x}$ Amplitude or peak value of x

$\tilde{x}$ Effective value of x

$\vec{x}$ Position vector

Symbols

α Coupling coefficient

η Modal displacements

κ Wavenumber

λ Wavelength

ν Poisson's ratio

Ω Computational domain

ω Angular frequency

$\partial\Omega$ Boundary of computational domain

Ψ Modal force

ρ Density

φ Phase offset

ζ Damping ratio

c Speed of sound

d Effective thickness

F External load

f Frequency

H Frequency response function

k Stiffness

L Sound pressure level

l Length

m Mass

p Pressure

S Periodic signal in frequency domain

s Periodic signal in time domain

T Period

t Time

v Damping coefficient

X System input

Y System output

Vectors and Matrices

$\boldsymbol{\eta}$ Transformed displacement vector

$\boldsymbol{\Phi}$ Modal matrix

$\boldsymbol{\Psi}$ Transformed loading vector

$\mathbf{A}$ State matrix

$\mathbf{B}$ Input matrix

$\mathbf{C}$ Output matrix

$\mathbf{D}$ Feedthrough matrix

$\mathbf{f}$ External load vector

$\mathbf{K}$ Stiffness matrix

$\mathbf{M}$ Mass matrix

$\mathbf{q}$ Displacement vector

$\mathbf{u}$ Excitation vector

$\mathbf{V}$ Viscous damping matrix

$\mathbf{x}$ State vector

$\mathbf{y}$ Output vector

Physics Constants

p_{ref} $2 \cdot 10^{-5}$ Pa, reference sound pressure

Contents

1. Introduction

This chapter explains the background to the problem that is to be solved, along with the aim and purpose of it. Moreover, the limiting factors are presented.

1.1 Background

Azelio is a Swedish company developing Stirling engine-based renewable energy solutions. One major challenge with renewable energy, such as wind and solar power is that the energy source is strongly varying in time. This makes it difficult to supply electricity at all hours. Especially at times when there is not much wind and no sun. To solve this problem, Azelio is developing a Thermal Energy Storing (TES) system that makes electricity from renewable sources accessible throughout the day [1].

Their idea is to store the overproduction of renewable power at certain hours as thermal energy. The overproduction is used to liquefy and heat an aluminium alloy with specific phase changing characteristics. During discharge, a heat transferring fluid transfers the thermal energy to a Stirling engine, which converts the heat to mechanical movement. Attached to the Stirling engine is a generator that converts mechanical movement to electricity. The Stirling engine, together with the generator and coolers constitutes the Power Conversion System (PCS).

The TES system consists mainly of three subsystems: A standard 40-foot steel container with a plywood floor, modified with openings and stiffeners. Two TES units, in which melted aluminium is stored and two PCS that converts thermal energy to electricity, see Figure 1.1. An empty TES unit weighs 1.5 tons while a filled one weighs 6 tons. The material data for steel, plywood and surrounding air are listed in Table 1.1.

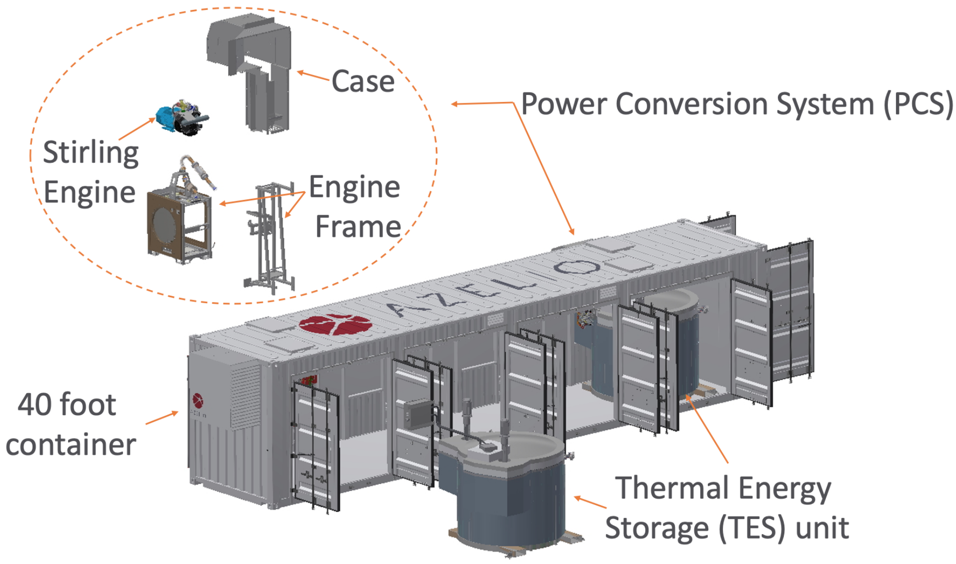

Figure 1.1: *Illustration of Azelio's TES system.*

Table 1.1: *Material data at 20 ^oC for steel, plywood and air obtained from [2]–[4].*

Material	Carbon Steel (S355J2)	Plywood (Keruing)	Air
Density [kg/m^2]	7,800	745	1.2041
Poisson's Ratio	0.29	0.49	-
Young's Modulus [GPa]	200	15.8	-
Yield Stress [MPa]	355	-	-
Speed of sound [m/s]	-	-	343.24

The container stands on ten levelling blocks that are placed on concrete, as seen in Figure 1.2. The TES units are kept inside the container for shelter against the ambient environment and the PCS's are attached on the outside. The heat transferring gas flows in a pipe between the TES unit and the PCS.

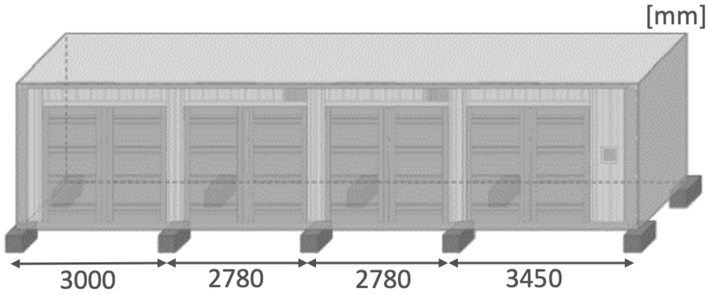

Figure 1.2: *The distance between the ten levelling blocks that the container stands on.*

The PCS consists of a Stirling engine with a generator, a cooler, a steel frame and a gas cooling system, see Figure 1.3. The Stirling engine is attached to the frame using four vibration isolating rubber mounts with 70 shore-A hardness[1] and a stiffness of approximately 1,900 kN/m. The entire PCS weighs about 650 kg.

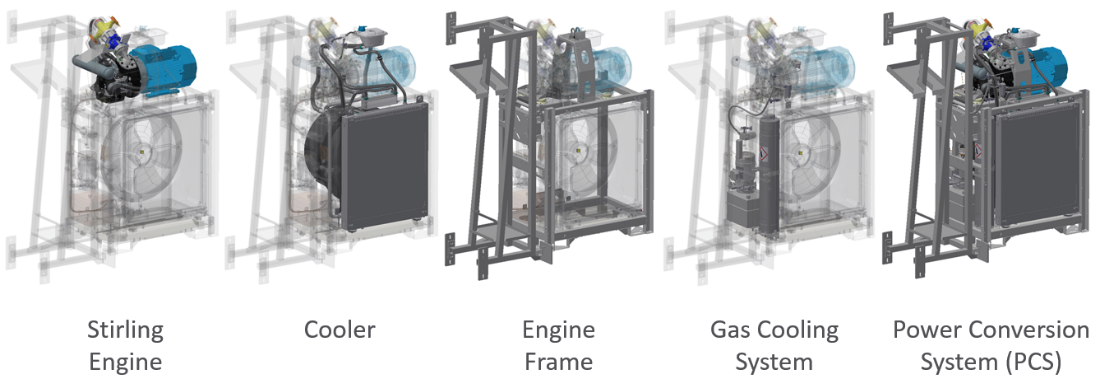

Figure 1.3: *Illustration of the different parts that are included in the PCS.*

The Stirling engine is an alpha type, shown in Figure 1.4. It has two cylinders, one warm expansion cylinder and one cold compression cylinder. The Stirling cycle starts with expansion of the working gas due to temperature increase caused by the heat transferring fluid [6]. The expansion starts in the warm cylinder and continues to the cold cylinder, which is 90^o behind the hot piston in its cycle. The gas reaches its maximum volume and

[1]Shore-A hardness is a measure of how much resistance a material has to indention [5]. A higher value indicates a harder material. The scale goes from 0 to 100.

moves to the cold cylinder where it is externally cooled by the gas cooling system, and the pressure drops. The cold piston, powered by a flywheel momentum, compresses the gas and the cycle is repeated. The crankshaft is attached to a generator which converts the rotation to electricity. The engine can be used at various constant revolutions per minute, rpm.

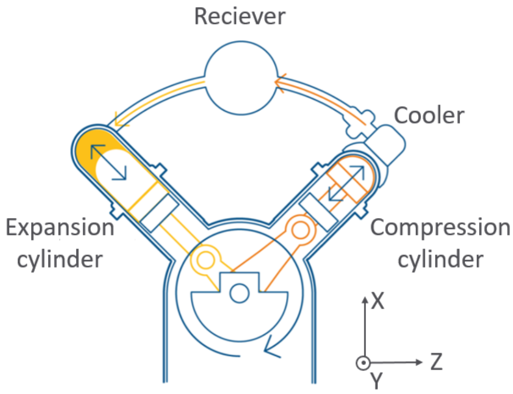

Figure 1.4: *Illustration of an alpha type Stirling engine used in the PCS.*

The crank motion cases free mass forces in the plane normal to the crankshaft and a torque about the crankshaft. The loads from Azelio's Stirling engine have been calculated in the centre point between the two bearings, seen in Figure 1.5. The loads were calculated at four discrete engine speeds between 1,250 and 2,000 rpm, corresponding to frequencies between 20.83 and 33.33 Hz. The load signals at each speed have been decomposed into their constituent frequencies. The constituent frequencies are known as engine orders and are integer multiples of the rotating frequency of the crankshaft. The first three orders, listed in Table 1.2, are dominating. The associated load data can be found in Appendix A. The free mass loads will make the engine vibrate, which causes sound to radiate from the TES system.

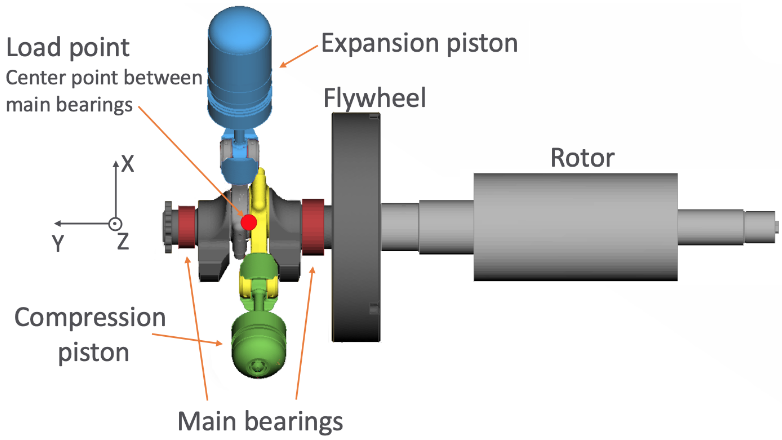

Figure 1.5: *The Stirling engine seen from above. The point where the imbalance loads are calculated at is marked in red in.*

Table 1.2: *Engine speeds and engine orders of Azelio's Stirling engine.*

Engine	**Engine Speed [rpm]**			
Order	1,250	1,500	1,750	2,000
1	20.83 Hz	25 Hz	29.17 Hz	33.33 Hz
2	41.67 Hz	50 Hz	58.33 Hz	66.67 Hz
3	62.5 Hz	75 Hz	87.5 Hz	100 Hz

1.2 Aim

The aim is to develop a numerical method that can be used to predict the exterior sound emitted by the TES system due to the vibrating Stirling engine, which can be applied to similar systems. Also, to perform measurements to validate the numerical model of the TES system.

1.3 Purpose

The TES system will be located in uninhabited areas, hence the sound level is not a problem under normal conditions. However, if the system would be serviced under operation, requirements regarding the noise level should be fulfilled. For this reason, the vibrations and sound level should be investigated.

The purpose is to develop a generic numerical method that can be used to predict exterior sound radiation. The method should be used as a tool during design evaluation to assess if a design fulfils the sound level requirements. The use of numerical tools at an early stage in the development process can save both time and money.

1.4 Limitations

To be able to fulfil the aim, the method being developed will be limited to analyse exterior sound that radiates due to structural vibrations that arise from the three first engine orders of the free mass loads induced by the Stirling engine. Other parts that may radiate sound from the system will be excluded. The sound will be analyzed at the far field located in a free field, which means that the sound waves will only propagate and not reflect against different objects.

The studied system is assumed to be linear and only the steady state of the system will be considered, thus the transient start-up will be out of scope. The method will be developed and verified for Azelio's TES system involving one Stirling engine, but should apply to similar systems.

The vibration tests are restricted to the demonstration unit located outdoors at Azelio's office in Åmål. Therefore, the system may be subjected to wind or rain, which can affect the results of the measurement. The number of points in which data can be collected is limited by the available equipment as well as the choice of test type. No tests will be performed when the engine is operating.

The numerical analysis will be done using the pre-processor ANSA v19.0.1, the solver

Ansys Mechanical Ansys Parametric Design Language (APDL) 2019 R3 and the post-processor META v20.1.0. Some results will be processed in Matlab R2020a.

2. Theory

In this chapter, the theory regarding linear structural dynamics is presented, such as modal and harmonic analysis, along with damping and Experimental Modal Analysis (EMA). Finally, some theory regarding acoustics and sound is described.

2.1 Equation of Motion

The equation of motion for a dynamic system is

$$\mathbf{M}\ddot{\mathbf{q}}(t) + \mathbf{V}\dot{\mathbf{q}}(t) + \mathbf{K}\mathbf{q}(t) = \mathbf{f}(t) \tag{2.1}$$

with $\mathbf{M}, \mathbf{V}$ and $\mathbf{K}$ being the mass, damping, and stiffness matrices, and $\mathbf{f}(t)$ is the external load vector [7]. The time-dependent accelerations, velocities, and displacements are denoted $\ddot{\mathbf{q}}(t)$, $\dot{\mathbf{q}}(t)$ and $\mathbf{q}(t)$. The equation of motion can be written on first order form by introducing a state vector $\mathbf{x}(t) = [\mathbf{q}(t)\ \dot{\mathbf{q}}(t)]^T$ and assuming that the mass matrix is symmetric and positive definite

$$\begin{cases} \dot{\mathbf{x}}(t) = \mathbf{A}\mathbf{x}(t) + \mathbf{B}\mathbf{u}(t) \\ \mathbf{y}(t) = \mathbf{C}\mathbf{x}(t) + \mathbf{D}\mathbf{u}(t) \end{cases} \tag{2.2}$$

where $\mathbf{y}(t)$ is the system response to a known system excitation $\mathbf{u}(t)$, and $\mathbf{A}, \mathbf{B}, \mathbf{C}$ and $\mathbf{D}$ are state-space matrices.

2.2 Modal Analysis

Modal analysis is a linear time-invariant analysis that gives information regarding mode shapes and natural frequencies of a system [7], [8]. In modal analysis, there is free vibration and damping is usually ignored. Therefore, the equation of motion (2.1) can be written like

$$\mathbf{M}\ddot{\mathbf{q}}(t) + \mathbf{K}\mathbf{q}(t) = \mathbf{0} \tag{2.3}$$

and the displacement $\mathbf{q}(t)$ can be expressed as

$$\mathbf{q}(t) = \mathbf{\Phi}_n e^{i\omega_n t} \tag{2.4}$$

where $\mathbf{\Phi}_n$ is the eigenvector representing the mode shape of the n:th natural frequency ω_n. Inserting the expression for the displacement into equation (2.3) and removing the time-dependency yields

$$[-\omega_n^2\mathbf{M} + \mathbf{K}]\mathbf{\Phi}_n = \mathbf{0} \quad n = 1, 2, ..., N \tag{2.5}$$

The expression is satisfied if $\mathbf{\Phi}_n = \mathbf{0}$ or if the determinant

$$|-\omega_n^2\mathbf{M} + \mathbf{K}| = 0 \tag{2.6}$$

which is of interest. From that equation, N different solutions can be determined for the angular natural frequency ω_n^2 and the mode shapes $\mathbf{\Phi}_n$. Usually, N are the modes of interest and are a fraction of the total number of Degrees of Freedom (DOF) of a system.

2.3 Frequency Domain Representation

A periodic signal $s(t)$ can be decomposed into a sum of sinusoidal components [9]. The component frequencies of the signal are called harmonics and are integer multiples of one fundamental frequency f_0. These are determined by computing the Fourier transform of the discrete, sampled signal, using a Discrete Fourier Transform (DFT). DFT is usually computed using Fast Fourier Transform (FFT), which transform the signal from the time domain to the frequency domain, see Figure 2.1. The magnitude at a given frequency is the amplitude of that frequency component and the argument is the phase offset.

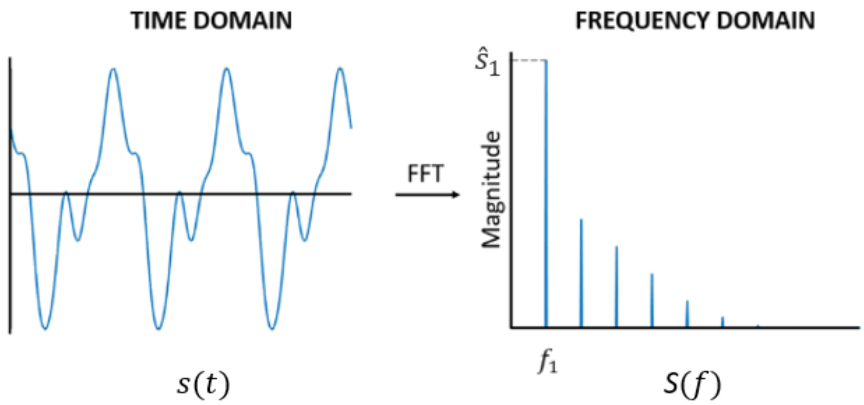

Figure 2.1: *Example of how FFTs a time signal $s(t)$ to a frequency signal $S(f)$. The magnitude $|S(f_n)|$ is the amplitude $\hat{s}_n$ and the argument $\angle S(f_n)$ is the phase φ_n of the n:th frequency component f_n.*

The sum of sinusoidal components that synthesizes the original periodic signal is called frequency domain representation. The frequency domain representation of a stationary harmonic signal $s(t)$ may be expressed as

$$s(t) = \sum_{n}^{N} \hat{s}_n \sin(2\pi f_n t + \varphi_n) \tag{2.7}$$

where f_n, $\hat{s}_n$ and φ_n are the frequency, amplitude and phase of the n:th component. To get an exact representation of the signal, an infinite number of components must be included. However, the components are usually of decreasing magnitude order and a sufficient accuracy can be achieved by including a finite number [10].

2.4 Harmonic Analysis

Harmonic analysis is based on the assumption that a stationary harmonic excitation gives a stationary harmonic response [7]. Let $\mathbf{f}(t)$ be a stationary harmonic load vector at angular frequency ω

$$\mathbf{f}(t) = \hat{\mathbf{f}} e^{i\omega t} \tag{2.8}$$

with complex-valued and time-invariant load amplitudes $\hat{\mathbf{f}}$. It follows from the harmonic assumption that the displacement response $\mathbf{q}(t)$ share the same harmonic behaviour and thus can be expressed as

$$\mathbf{q}(t) = \hat{\mathbf{q}}e^{i\omega t} \tag{2.9}$$

with complex-valued and time-invariant displacement amplitudes $\hat{\mathbf{q}}$. Inserting the expressions into the equation of motion (2.1) and removing the common time-dependency yields

$$\Big[-\omega^2\mathbf{M} + i\omega\mathbf{V} + \mathbf{K}\Big]\hat{\mathbf{q}} = \hat{\mathbf{f}} \tag{2.10}$$

The complex displacement amplitudes $\hat{\mathbf{q}}$ may be computed using the mode-superposition method or directly using the full method [11]. In the full method, the whole system matrices are used to compute the harmonic response. In this method, there is no reduction of the system and the matrices can be symmetric or unsymmetrical, which means that this method may be computationally expensive. The mode-superposition method is discussed in the next section.

If the harmonic load contains several sinusoidal components, as described in Section 2.3, the total response is computed by adding the contribution from each component n, using the superposition principle [7]. By expressing the complex amplitudes $\hat{q}$ on polar form with amplitude $\hat{q}^*$ and phase φ, the superposition principle is defined as

$$\hat{q}(t) = \sum_{n=1}^{N_h} \hat{q}_n^* \sin(2\pi f_n t + \varphi_n) \tag{2.11}$$

where $\hat{q}_n^*$ is the amplitude and φ_n is the phase of the n:th component. N_h is the total number of components in the harmonic load signal.

2.4.1 Mode-Superposition Method

The mode-superposition method uses the results from the modal analysis to determine the dynamic response of a system subjected to harmonic or transient excitation [12]. Thus, it enables a faster solution method compared to the full method [11]. The method is based on the assumption that the harmonic or transient displacement $\mathbf{q}(t)$ can be written as a linear combination of the eigenmodes $\mathbf{\Phi}_n$

$$\mathbf{q}(t) \approx \sum_{n=1}^{N} \eta_n(t)\mathbf{\Phi}_n \tag{2.12}$$

where η_n are modal displacements [7]. The relation would be exact if all eigenmodes of the system were used, but that is rarely the case due to computational cost [13]. Generally, eigenmodes up to a certain frequency are solved. For instance, eigenmodes up to 2.5 times the maximum frequency of interest are included in the analysis.

Equation (2.12) can be written on matrix form by collecting the modal DOF in a column vector $\boldsymbol{\eta}$ and the eigenmodes in a rectangular modal matrix $\mathbf{\Phi}$ in which each column represents an eigenmode [7]

$$\mathbf{q} = \mathbf{\Phi}\boldsymbol{\eta} \tag{2.13}$$

Inserting the expression in the equation of motion (2.1) and pre-multiplying with $\mathbf{\Phi}^T$ yields

$$\mathbf{\Phi}^T\mathbf{M}\mathbf{\Phi}\ddot{\boldsymbol{\eta}} + \mathbf{\Phi}^T\mathbf{V}\mathbf{\Phi}\dot{\boldsymbol{\eta}} + \mathbf{\Phi}^T\mathbf{K}\mathbf{\Phi}\boldsymbol{\eta} = \mathbf{\Phi}^T\mathbf{f}(t) = \mathbf{\Psi}(t) \tag{2.14}$$

Due to the orthogonality-property of the eigenmodes, $\mathbf{\Phi}^T\mathbf{M}\mathbf{\Phi}$ and $\mathbf{\Phi}^T\mathbf{K}\mathbf{\Phi}$ only has non-zero elements on the diagonal [7], [14]. Through mass matrix normalization, the eigenmodes are scaled such that $\mathbf{\Phi}^T\mathbf{M}\mathbf{\Phi} = \mathbf{I}$ and $\mathbf{\Phi}^T\mathbf{K}\mathbf{\Phi} = \mathrm{diag}(\omega_n^2)$. By only allowing damping that is proportional to stiffness and mass, the damping matrix is also diagonal. Thus, the problem can be simplified as

$$\ddot{\eta}_n + 2\omega_n\zeta_n\dot{\eta}_n + \omega_n^2\eta_n = \Psi_n \quad n = 1, ..., N \tag{2.15}$$

where Ψ_n is modal force and ζ_n is damping ratio for mode n. The coupled equation system in equation (2.14) is by the transformation converted into a decoupled system. This reduces the number of equations from the system's number of DOF to a fraction N. The individual modal responses η_i are superimposed using equation (2.12) to get the actual displacement response. The concept of mode-superposition is illustrated for a simply supported beam in Figure 2.2. Any displacement shape can be represented by a sum of a sufficiently large number of modes.

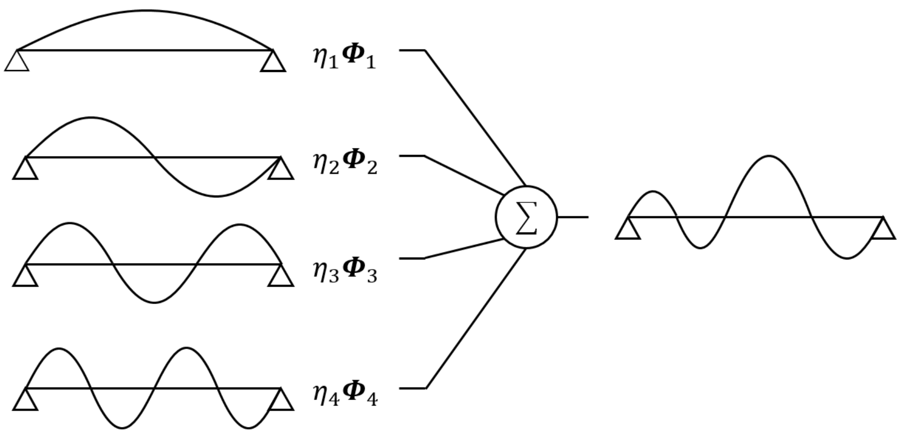

Figure 2.2: *Schematic illustration of the concept of mode-superposition. The total response of the system is computed by adding fractions η_n of each mode shape $\boldsymbol{\phi}_n$.*

2.5 Frequency Response Function (FRF)

The frequency dependent transfer function $H(\omega)$ from a system input excitation $X(\omega)$ to an output response $Y(\omega)$ is called the system's Frequency Response Function (FRF) [15]

$$H(\omega) = \frac{Y(\omega)}{X(\omega)} \tag{2.16}$$

The response can be described in terms of displacement, velocity or acceleration. The corresponding FRFs are called receptance, mobility and accelerance. All of these are mathematically related and the measure of one can be used to calculate the others [16]. Accelerance is generally the preferred measured response since the most convenient motion transducer is the accelerometer.

In EMA, FRFs are used to identify a system's modal parameters [17]. Figure 2.3 displays an example of what a FRF can look like. From the curve, the natural frequencies, modal damping and mode shapes of the system can be identified. The peaks correspond to natural frequencies and the width of the peaks is proportional to the modal damping. The mode shape can be determined using the amplitude and phase of multiple FRFs.

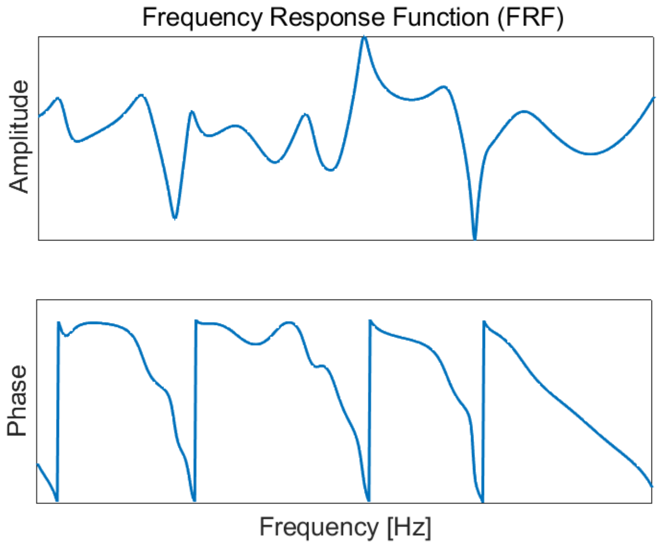

Figure 2.3: *An example of a Frequency Response Function (FRF). A FRF gives the relation between an input and an output. The peaks in the amplitude plot represents natural frequencies.*

2.6 Damping

In a numerical modal analysis, damping is often neglected. This, however, is not the case in harmonic analysis. Damping is the phenomenon when mechanical energy is dissipated into internal thermal energy or other damping mechanisms in a dynamic system [18]. There are several types of damping present in a system: structural, internal, and fluid damping. Since there are different types, a good insight into the physics is required to get the correct damping of a model [7].

The damping ratio ζ describes how rapidly the oscillations decay from one cycle to the next in a vibrating system [19]. The relation of the damping ratio can be obtained from the actual and critical damping v and v_c as

$$\zeta = \frac{v}{v_c} \tag{2.17}$$

with the critical damping coefficient being $v_c = 2\sqrt{km}$. Thus,

$$\zeta = \frac{v}{2\sqrt{km}} = \frac{v\omega_n}{2k} \tag{2.18}$$

where m is the mass, k is the stiffness and ω_n is the angular natural frequency.

A system can be undamped ($\zeta = 0$), underdamped ($\zeta < 1$), critically damped ($\zeta = 1$)

or overdamped ($\zeta > 1$), see Figure 2.4a. For an undamped system, the object would continue to oscillate infinitely long and the frequency response peaks would be infinitely large, see Figure 2.4b. This is rarely the case in reality, however, the damping can be so small that it is practically negligible. In an underdamped system, the oscillations will decrease until the system comes to rest. The smaller the damping ratio is, the longer it will take until the vibrations have stopped. A critically damped system will go back to its equilibrium position in an exponential rate without any oscillations. If the system is overdamped, it will slowly return to its initial position without overshooting.

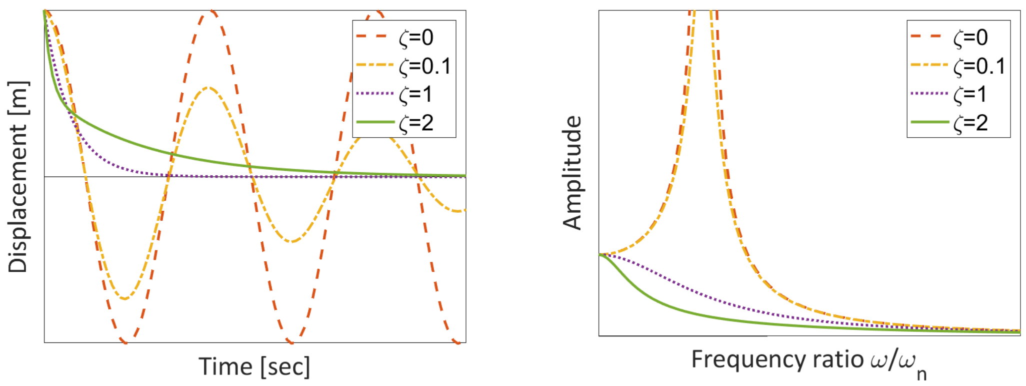

(a) *Oscillations* ***(b)*** *Amplitude*

Figure 2.4: *The figures show an undamped ($\zeta = 0$), underdamped ($\zeta < 1$), critical damped ($\zeta = 1$) and overdamped cases ($\zeta > 1$) and how that affects the oscillation and amplitude.*

The damping ratio ζ can be computed from a FRF using the half power bandwidth method

$$\zeta = \frac{f_2 - f_1}{2 \cdot f_n} \tag{2.19}$$

where f_n is the natural frequency and f_1 and f_2 are the frequencies 3 dB down from the peak value to the left and right of the natural frequency, respectively, see Figure 2.5 [18]. This means that a wider peak will result in higher damping.

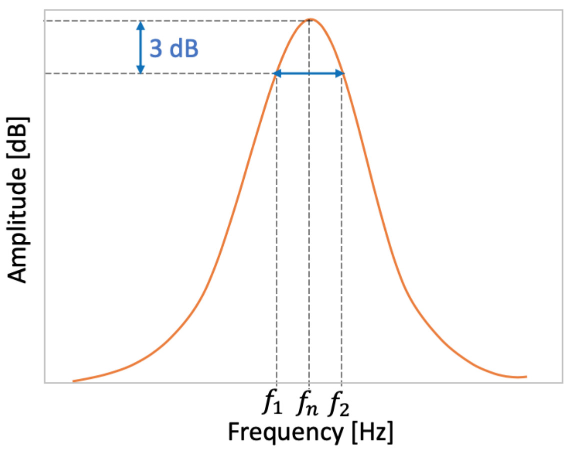

Figure 2.5: *The half power bandwidth method to compute the damping.*

2.7 Experimental Modal Analysis (EMA)

EMA is useful to determine a structure's dynamic properties in terms of natural frequencies, damping and mode shapes [20]. Besides, EMA can be used to validate a Finite Element (FE) model and calibrate it, if the results between the two methods do not coincide.

In EMA, the relationship between a forced measured excitation and the vibration response at certain points on a structure is established [21]. The relationship is expressed in terms of FRF.

2.7.1 Equipment

To perform an EMA, a transducer, an excitation mechanism and a Data Acquisition (DAQ) system are required [7], [22]. A transducer, usually an accelerometer, can measure the response from the excitation in terms of acceleration. These are often used due to their high sensitivity and low cost.

The excitation mechanism can, for instance, be an impact, snap-back or a shaker. For the impact test, a force sensor hammer is excited with an impulse. For good repeatability in tests, the hammer needs to be struck on the same excitation point with the same angle of attack. The force is measured in a load cell that is attached to the hammer's head. Depending on the size of the structure, different sizes of the hammer can be used. This test method is quick to execute, but the results may lack in accuracy since it can be difficult to differentiate the response from noise.

With the snap-back test, the structure is also excited with an impulse. In the snap-back test, a stress is applied to the structure by attaching a known weight to a point on the structure and releasing it. Releasing the weight will give a known excitation force. This test method is not as quick as the impact hammer test. However, it gives better repeatability and can be used on larger structures.

An alternative is to use a shaker, for which the structure can be excited with different kinds of controlled input signals, such as a sinusoidal one. Therefore, it is possible to directly identify the mode shape. This excitation mechanism will give higher accuracy since noise can be reduced. However, this equipment can be more expensive than the other excitation mechanisms. Furthermore, it is more time consuming to set up the equipment for the shaker test.

To store the measured excitation and response signals, a DAQ system is required. DAQ converts analogue data to digital. Software that uses FFT is also necessary to be able to compute FRFs.

2.8 Acoustics

Acoustics is the branch in physics that deals with generation, propagation and reception of vibrations and sound in mediums such as gases, fluids or solids [23]. Sound is detected when there is a rapid change in pressure above and below the static ambient pressure of the medium [15]. A sound pressure wave caused by a noise source can be described by a sinusoidal function of time

$$p(t) = \hat{p}\sin(2\pi f t + \varphi) \tag{2.20}$$

with frequency f, amplitude $\hat{p}$ and phase φ [15]. The sound wave moves with speed c. During one period $T = 1/f$, the wave has spread a distance λ, known as the wavelength

$$\lambda = cT = \frac{c}{f} \tag{2.21}$$

The frequency and the wavelength are inversely proportional to each other. If the frequency is large, the wavelength is short, and vice-versa.

2.8.1 Acoustic Fields

The acoustic field around a noise source can be divided into two parts; near field and far field [24]. The field within two wavelengths from the vibrating noise source is called near field. Near the noise source, waves will fluctuate back and forth without propagating and no relation between pressure and distance can be established. Further away from the source, the near field diminishes and the sound is dominated by waves that propagate, see Figure 2.6. The fluctuating to propagating behaviour will be mixed until a distance of two wavelengths is reached, where the fluctuating part practically vanishes. This is where the far field begins. From this distance and forward, the sound will strictly propagate and the noise source can be treated as a point source in three dimensions. A relation between pressure and distance can be established, where the sound pressure drops 6 dB for each doubling distance away from the source. A single sound recording microphone will give reliable and predictable results. Therefore, it is preferable to make sound level measurements in the acoustic far field.

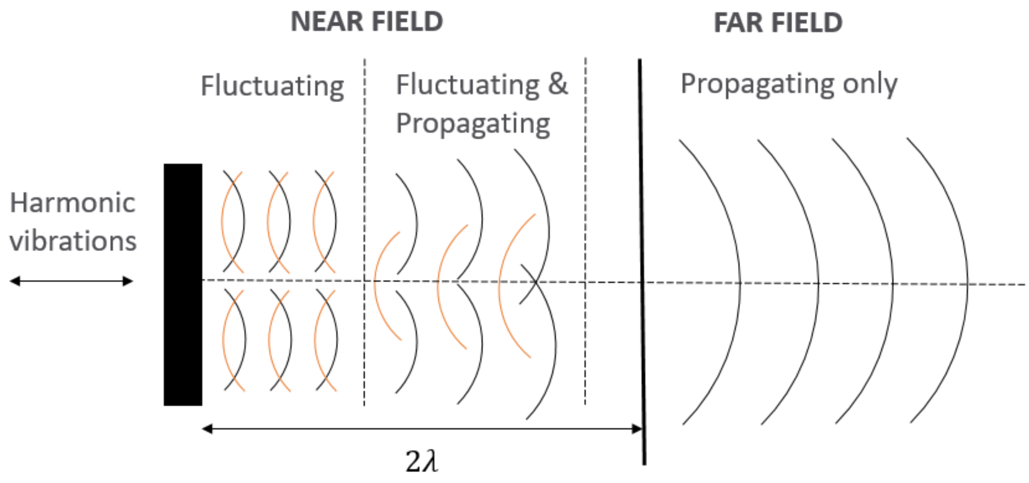

Figure 2.6: *Example of the acoustic near field and far field. The noise source is a harmonically vibrating plate.*

2.8.2 Sound Pressure Level

The level of sound is measured as the sound pressure level in decibel (dB) with a sound pressure microphone [15]. The sound pressure level L is defined as

$$L = 10 \cdot \log\left(\frac{\tilde{p}^2}{p_{ref}^2}\right) \tag{2.22}$$

where $p_{ref} = 2 \cdot 10^{-5}$ Pa is the reference sound pressure and $\tilde{p}$ is the effective pressure that can be defined in terms of amplitude as $\tilde{p} = \hat{p}/\sqrt{2}$. The sound pressure level can be weighted according to an A-weighting filter, see Figure 2.7, which accounts for how the human ear responds to sound [25]. The weighted sound pressure levels are labelled as dB(A). The A-weighting curve ranges from 20 to 20,000 Hz, which is the maximum audible range of sound for humans. The audible frequency range can vary between individuals and the hearing of higher frequencies is lost with age [26]. In the Figure, it can be seen how an average human is most sensitive to sounds between 2,000 to 5,000 Hz and less sensitive to sounds with lower or higher frequencies [27]. In the sensitive range, the volume does not have to be as loud for the human to perceive the sound.

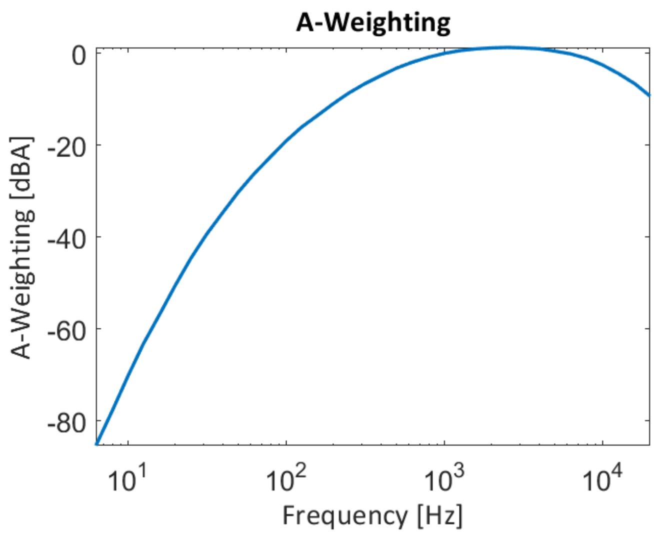

Figure 2.7: *Displays an A-weighting curve. Data is obtained from [28].*

The sound pressure level of different frequency components can be added according to

$$L_A = 10 \cdot \log \sum_{n=1}^{N} 10^{(L_n + \Delta A_n)/10} \tag{2.23}$$

where L_n is the sound level of frequency component n and ΔA_n is the A-weighting from Figure 2.7 [15].

2.8.3 Governing Equations

The acoustic wave equation describes the propagation of acoustic waves through a medium [15]. The homogeneous linearized wave equation for sounds in fluids, called the Helmholtz equation, is derived from the Navier-Stokes equation along with the ideal gas law and the flow continuity equation using the following assumptions:

(i) The medium is homogeneous and isotropic, thus it has the same properties in all points and directions.
(ii) The medium is linear elastic, which means that Hooke's law is valid.
(iii) The viscosity is negligible.
(iv) Heat transfer by convection is negligible and all processes are assumed to be adiabatic.
(v) Body forces, like gravitation, are neglected. Hence, the pressure and density of the medium are assumed to be constant.
(vi) The pressure disturbances are small, which enables linearization of equations.

This yields the homogeneous wave equation describing sound pressure evolution in a fluid

$$\frac{\partial^2 p}{\partial t^2} - c^2 \nabla^2 p = 0 \tag{2.24}$$

where ∇^2 is the Laplace operator, c is the speed of sound in the fluid and $p(\vec{x}, t)$ is the acoustic pressure in a certain point $\vec{x}$. Any source term is added to the right-hand side of the equation.

Wave propagation in free space due to a source $F(\vec{x}, t)$ is modelled by the inhomogeneous Helmholtz equation [29]. The derivation of the equation is based on the assumption that a harmonic source $F(\vec{x}, t) = \hat{F}(\vec{x})e^{-i\omega t}$ generates harmonic waves with the same frequency of oscillations ω, as $p(\vec{x}, t) = \hat{p}(\vec{x})e^{-i\omega t}$. Inserting these expressions in the wave equation (2.24) and removing the common time-dependency yields the inhomogeneous Helmholtz equation

$$\nabla^2 \hat{p}(\vec{x}) + \kappa^2 \hat{p}(\vec{x}) = \hat{F}(\vec{x}) \tag{2.25}$$

where $\kappa^2 = \omega^2/c^2$ is a constant called wavenumber. The solution to the equation is different for interior and exterior problems [29]. In interior problems, equation (2.25) is defined in a bounded domain Ω with associated Boundary Conditions (BC), such as Dirichlet or Neumann conditions, see Figure 2.8a. In exterior problems, such as scattering problems, equation (2.25) is defined in an unbounded domain outside Ω, see Figure 2.8b. In exterior problems, there is no source, $\hat{F} = 0$. Instead, the waves are generated by inhomogeneous BCs on $\partial\Omega$.

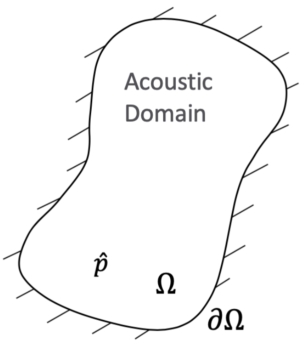

(a) *Interior problem*

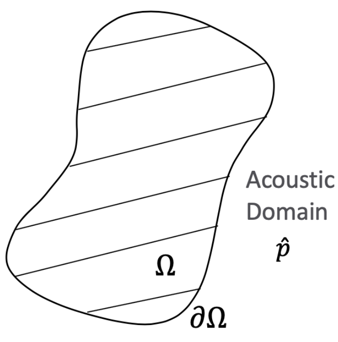

(b) *Exterior problem*

Figure 2.8: *The acoustic domain. Equation* (2.25) *is set inside* Ω *in interior problems and outside* Ω *in exterior problems.*

2.8.4 Numerical Methods

There exist several numerical methods for solving the Helmholtz equation. For instance, the Finite Element Method (FEM), the Boundary Element Method (BEM) or Wave Based Technique (WBT). Different software uses different techniques.

In FEM, the entire domain is discretized into elements and nodes. FEM is useful in interior acoustics and lower-frequency problems [4]. For an increasing domain size or frequency, the number of DOF will increase exponentially, making the model larger and the computational time longer. Although FEM is advantageous to use for interior acoustics, it can also be used for exterior acoustics. Both pressure- and displacement-formulated elements can be used to analyse acoustics. The most commonly used is pressure-formulated.

BEM is advantageous for problems with large or infinite domains, such as exterior sound radiation [30]. In BEM, only the boundary of the domain has to be discretized. Thus, the dimension of the problem is reduced. This means lower computational cost, less pre-processing time and less unwanted information [31]. The partial differential equation in equation (2.25) is re-formulated to a boundary integral equation and an integral that relates the boundary solution to the solution at points in the domain. After solving the boundary integral approximately through discretization, the solution at any arbitrary point of the domain can be found.

WBT gives an exact solution inside the domain, compared to element based methods that approximate the solution using shape functions [32]. WBT can be used to solve high-frequency problems since the model size is not dependent on the frequency range as it is for the element based methods. However, in WBT the boundary conditions might be violated.

2.8.5 Coupling

In an acoustic analysis, both the vibrating source and the medium itself is considered. The fluid and structural domains can be solved separately, or simultaneously in a Fluid-Structure Interaction (FSI) [4]. FSI is based on the assumption that the structure and fluid are affected by one another in a two-way coupling. Another way to solve an acoustic analysis is by using one-way coupling, where it is assumed that only the fluid is affected by the structure or the other way around [33]. In this solution method, the analysis is either done on the structure or the fluid first and then the results are given as an input in the other analysis. Solving the problem with one-way coupling reduces the problem and is faster while FSI will give a more accurate result [34]. For both FSI and one-way coupling, the interface between the fluid and structure has to be defined since this is where the information is shared between the different domains. To decide which solution method to be used, the coupling coefficient α can be computed at a certain angular frequency $\omega = 2\pi f$ as

$$\alpha = \frac{c\rho_{fluid}}{\omega d\rho_{solid}} = \frac{c\rho_{fluid}}{2\pi f d\rho_{solid}} \tag{2.26}$$

where ρ_{fluid} and c are the density and speed of sound of the fluid, while ρ_{solid} and d are the density and the effective thickness of the solid [33]. If the coupling coefficient is less than one, one-way coupling can be assumed. Otherwise, FSI should be used.

3. Method

In this chapter, the method that was used to simulate exterior sound radiation from the TES system is described. First, a structural FE-model of the system was created, which modal and harmonic analyses were executed on. The modal Finite Element Analysis (FEA) gave information regarding placements of accelerometers for the EMA. When the EMA had been performed, the measured data were processed to obtain a structural damping that could be used in the FE-model of the structure. An exterior acoustic simulation could then be computed using the structural vibrations from the harmonic FEA as a BC to generate sound pressure waves in the acoustic domain.

3.1 Structural FE-Model

Existing models of the TES system and its components were supplied by Azelio. These were modified in Ansa and Ansys Mechanical APDL to create a FE-model of the TES system. Some existing parts were modified, such as removing the small radius at plate corners to enable a larger element size. Parts that were assumed to neither contribute with stiffness nor radiate sound were excluded, such as the ventilation shaft and the case of the PCS. Some parts were added, for instance, door hinges and locking mechanisms to get a more realistic response of the doors. The structural FE-model can be seen in Figure 3.1. The container stands on ten levelling blocks. The distance between each block can be seen in Figure 1.2. The associated nodes on the bottom of the container floor in the structural FE-model were fixed in all six DOF.

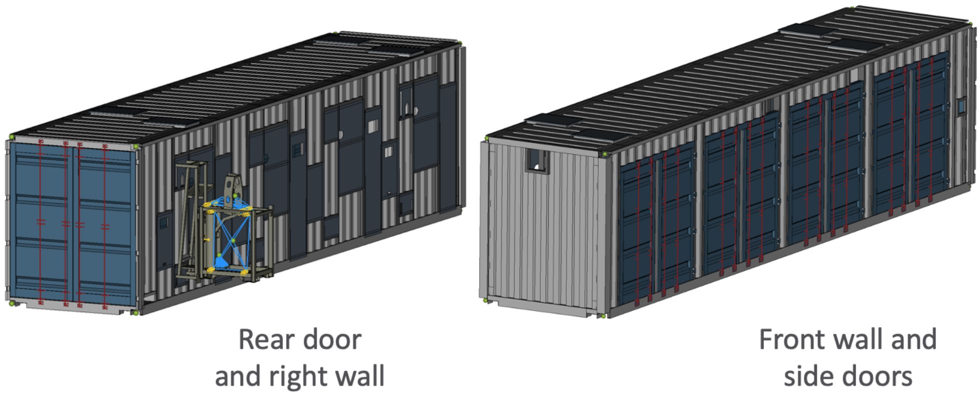

Figure 3.1: *The illustration shows the structural FE-model of the TES system.*

The model consists of about 700,000 DOF and is constructed with roughly 110,000 elements of six different types: shell, mass, beam, spring-damper, target and contact elements. The model is mainly constructed with first-order shell elements. The size of the elements is controlled by the frequency of the structural vibrations. It is recommended to use six to ten elements per wavelength to resolve a wave, with the shortest wavelength λ_{min} governing the element size [35]. According to equation (2.21) in Section 2.8, the highest frequency has the shortest wavelength, whereby

$$\lambda_{min} = \frac{c}{f_{max}} = \frac{343.24}{2.5 \cdot 100} \approx 137 \text{ cm} \tag{3.1}$$

The speed of sound in air c, was obtained from Table 1.1. The maximum frequency f_{max} is 100 Hz and corresponds to the third engine order at 2,000 rpm, see Table 1.2. The FE-model will be used in a harmonic analysis using mode-superposition. As mentioned in Section 2.4.1, that requires eigenmodes and frequencies up to 2.5 times the maximum exciting frequency. Therefore, f_{max} was multiplied with 2.5. The maximum allowed element size l_e was computed using nine elements per wavelength $N_{e,w}$ as

$$l_e = \frac{\lambda_{min}}{N_{e,w}} = \frac{137}{9} \approx 15 \text{ cm} \tag{3.2}$$

This element size was used for the majority of the model. The existing model of the PCS had a finer mesh of 2 cm elements, which was kept due to its complex geometry that a coarser mesh would not be able to capture.

Mass elements were created in the Centre of Gravity (COG) of several parts that were assumed to act as rigid bodies. The location and weight of the mass elements can be seen in Figure 3.2. Since the acoustic analysis will be limited to only consider the vibrations from one Stirling engine, only one PCS was modelled. Its corresponding TES unit was modelled as filled and the other one as empty.

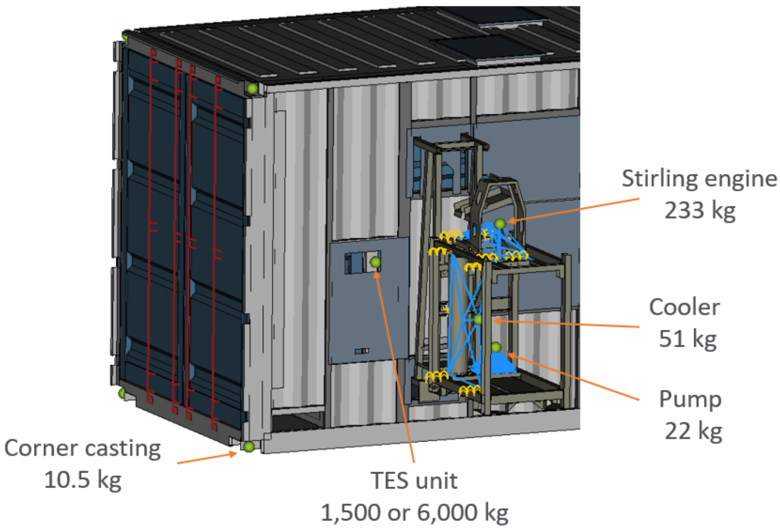

Figure 3.2: *Location and weight of the mass elements used in the structural FE-model. An empty TES unit weighs 1,500 kg while a filled weighs 6,000 kg.*

The mass elements used on the corner castings were connected to the system with rigid connections. The rest of the mass elements were connected to the structure using mass-less beam elements. Beams were also used to model screws, screw holes, hinges and door locks. Moreover, the point in which the free mass loads acts, see Figure 1.4, was connected to the PCS with beam elements.

Spring-damper elements were utilized to model the engine mounts and the attachment of the cooler to the PCS. The stiffness of the cooler attachment had already been defined as 750 kN/m in the existing model of the frame and was not changed. The engine mounts were modelled with both stiffness and damping. The stiffness was set to 1,900 kN/m based on data from the supplier, see Section 1.1, and the viscous damping v was estimated from equation (2.18) as

$$v = \frac{2\zeta k}{\omega_{mean}} = \frac{2\zeta k}{2\pi f_{mean}} = \frac{2 \cdot 0.15 \cdot 1.9 \cdot 10^6}{2 \cdot \pi \cdot 60.4} \approx 1,503 \text{ kg/s} \tag{3.3}$$

where the damping ratio ζ was assumed to be 15 % and the mean excitation frequency f_{mean} is 60.4 Hz, see Table 1.2. A damping ratio of 15 % was chosen since that is what Schiavi and Prato obtained in a resonant frequency response test for rubber of 66 shore-A hardness [36], which is close to the 70 shore-A hardness of the engine mounts.

Contact between parts was modelled with the Augmented Lagrangian method[1] as sliding or bonded, edge-to-face or face-to-face contacts. The sliding contact was chosen on parts that are not connected but are in contact and the bonded contact was used on parts that were screwed or welded together. In contacts between two faces, the two surfaces form a contact pair. One surface is constructed with target elements and the other with contact elements. The pairs are in contact if a certain sphere radius, centred around the integration point of the contact element, is within the target surface. The size of the region is directly influencing the computational cost. Therefore, in the majority of the contacts, a radius of 2 cm was used. Because of this, two integration points were used for all elements to be able to detect face-to-face contacts for pairs where the elements almost did not align.

The whole TES system, except the plywood container floor, was modelled with steel using the material data in Table 1.1. Since all parts of the PCS were not included in the model, the density of the engine frame was modified from 7,800 to 12,350 kg/m^2 to get a total mass of 650 kg, which corresponds to its actual weight mentioned in Section 1.1. The bottom plate of the engine frame is in reality grating but was modelled with sheet metal. To account for the lower mass of grating, the density was set to one-third of the density of steel.

3.2 Modal Analysis

A modal analysis of the TES system was performed in Ansys Mechanical APDL, where the damping and any nonlinearities, such as plasticity or contact elements were ignored. The software offers four methods to solve the symmetric eigenvalue problem; the Block Lanczos Method, the Preconditioned Conjugate Gradients (PCG) Lanczos Method, the Supernode Method and the Subspace Method [38]. Different methods are to be used for different problems. To decide which eigensolver to use, an efficiency test was performed. The results can be seen in Figure 3.3. From the Figure, it can be seen that the Block Lanczos method and the Subspace method are most efficient, independently of the number of modes that were extracted. However, the Subspace method works best for well-shaped elements, which the model does not necessarily consist of [39]. Therefore, Block Lanczos

[1] Augmented Lagrangian method solves constrained problems, such as contact, by replacing it with unconstrained problems and adding a Lagrangian multiplier estimate at each iteration [37].

method was chosen.

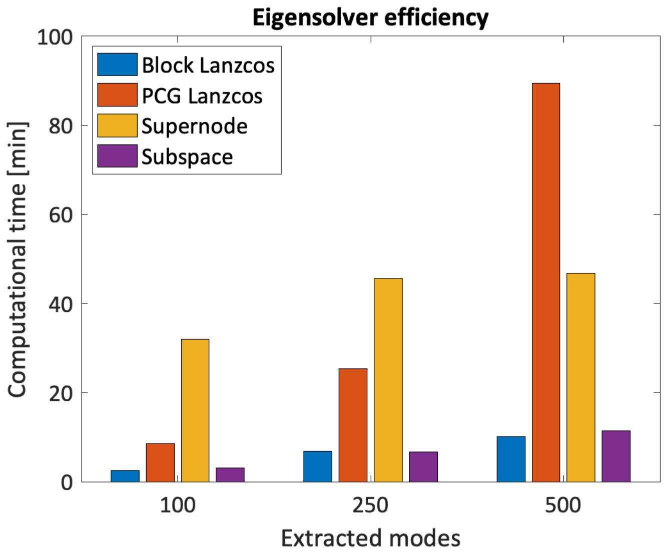

Figure 3.3: *The computational time for different eigensolver methods.*

After selecting an eigensolver, 897 mode shapes and natural frequencies were extracted to get modes ranging up to 2.5 times the maximum exciting frequency of 100 Hz, see Table 1.2. This gave modes ranging from 0 to 250 Hz. The results from the modal analysis are required as input for the mode-superposition harmonic analysis. Furthermore, the results could be used to decide where to place the motion transducers on the TES system in the EMA.

3.3 EMA of the TES System

EMA can be divided into three constituent parts; test planning, frequency response measurement and parameter identification through signal processing. An EMA was executed to investigate the dynamic behaviour of the TES system, intending to extract information regarding the structural damping and the vibration isolation properties of the engine mounts[2]. Furthermore, to validate the structural FE-model in terms of dynamic response.

3.3.1 Test Planning

A test plan was constructed to save time during the test day and to increase the possibility of obtaining a successful result. The preparation involved several steps: choosing an excitation method and a motion transducer, testing the equipment and finding locations to measure the response.

Various methods can be used to excite the system. For this test, the impact hammer was chosen to ensure that enough data could be collected without largely affecting the quality of the result. The hammer can be seen in Figure 3.4a. A second option was to use the snap-back test if the hammer would not give enough response. This was not chosen as the preferred method since it would be difficult to find an excitation point on the TES

[2]Vibration isolation mounts reduce the transmission of vibration, they do not necessarily damp the vibrations.

system to perform this test. It would take more time to repeat the test compared to the hammer test and more equipment, such as a pulley, would be needed to be able to excite the TES system horizontally. The shaker test was not considered due to the size of the structure and since the available equipment for this test was cumbersome and inadequate.

Accelerometers were chosen to measure the response in various points on the TES system. Both uniaxial and triaxial accelerometers were available. Considering that the TES system mainly consists of large panels whose response will be normal to the surface, uniaxial accelerometers were chosen. A picture of a uniaxial accelerometer can be seen in Figure 3.4b. Furthermore, the signal from the accelerometers and the actuator was processed using a DAQ system with four channels, see Figure 3.4c. This means that three uniaxial accelerometers can be used to measure the response in each configuration, compared to one triaxial accelerometer that would take up three out of four channels. The accelerometers will be attached using beeswax. If that is not enough, the attachment will be supplemented with electrical tape.

(a) *Impact hammer* ***(b)*** *Accelerometer & cable* ***(c)*** *DAQ system*

Figure 3.4: *Some of the test equipment used in an impact hammer test.*

The equipment required to perform an impact hammer test was borrowed from Chalmers University of Technology and consists of:

- Hammer with an attached weight
- Three uniaxial accelerometers
- DAQ system with four channels
- Computer with DAQ toolbox in Matlab
- Extension cables
- Beeswax
- Electrical tape

As can be seen in Figure 3.4a, the available hammer is rather small. Because it was uncertain if the impact hammer would be enough to excite the system, equipment for performing a snap-back test would also be brought at the test day.

3.3.1.1 Trial EMA

A trial EMA was performed at Chalmers University of Technology prior to the test to get familiar with the equipment to be used and to construct a test procedure. Both the impact hammer test and the snap-back test were executed on a spring attached to the ceiling with rubber bands. This test object was chosen since its dynamic behaviour was known, even though it differs from the TES system. Therefore, the test execution, equipment and signal processing could be validated.

3.3.1.2 Test Plan

With the purpose of the experiment in mind, a test plan was prepared based on the trial EMA and results from the modal FEA. The EMA would consist of three sub-tests: a vibration isolation test, a structural response test and a direct mobility test.

A vibration isolation test would be done on the rubber engine mounts to get information regarding their vibration isolation properties. The characteristics of the mounts are of interest since they play an important role in the dynamic behaviour of the system and since no information could be obtained from the manufacturer. In a vibration isolation test, the response is measured on the source and receiver side of the insulator, which corresponds to the upper and lower side of the engine mount [15]. The engine mount is excited on the source side, where the engine is mounted. An illustration of the vibration isolation test of an engine mount can be seen in Figure 3.5. The difference in response between the source and receiver gives information regarding the isolating properties of the mount.

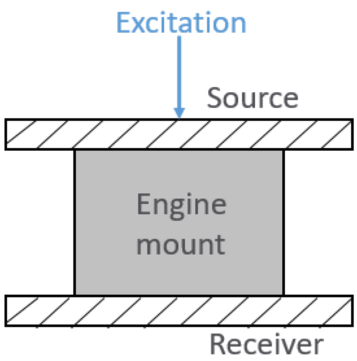

Figure 3.5: *The figure illustrates a vibration isolation test of an engine mount. The response is measured at the source and receiver side of the engine mount. The excitation is on the source side.*

The structural response test would aim at extracting a global structural damping that can be used in the structural FE-model. Also, the results will be compared to FEA to validate the structural FE-model. In the structural response test, the system is excited near the vibrating source, in this case the Stirling engine, and the response is measured in multiple points on the structure. Therefore, it was necessary to prepare a proposal of where to place the accelerometers. The proposal was constructed based on the modal FEA. Points that were moving a lot, close to the Stirling engine, and in many modes were chosen as candidates. These can be seen in Figure 3.6. The corner of the container was chosen as a control point since it is very stiff and should not move when the TES system is excited. No points on the roof were chosen, even though many modes could be detected there, because of difficulties in getting the correct equipment to safely measure the response there.

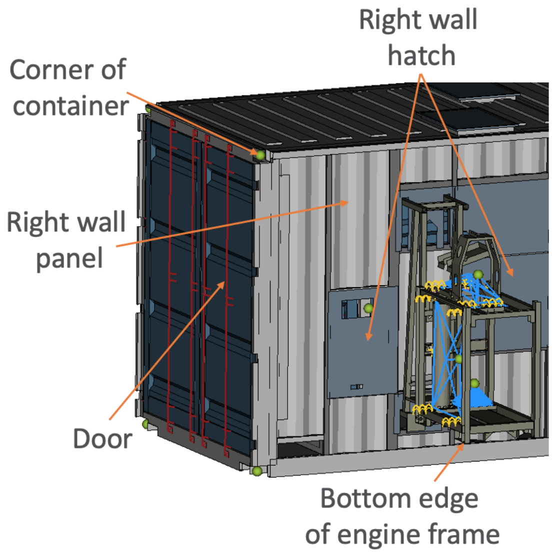

Figure 3.6: *A proposal of where to place the accelerometers in the structural response test.*

In a direct mobility test, the impact force and the structural response is measured in the same point [40]. The direct mobility test would be performed to obtain information regarding an individual damping of parts that have isolated modes. An isolated mode is a mode where a single part moves, independently, without affecting the rest of the system. Therefore, it was of interest to identify isolated modes in the TES system prior to the test. In the modal FEA, such modes were identified at the front wall of the container and the engine frame, see Figure 3.7. The accelerometer would be placed at the bottom of the engine frame, a place that could be accessed in reality, and at the middle of the front wall.

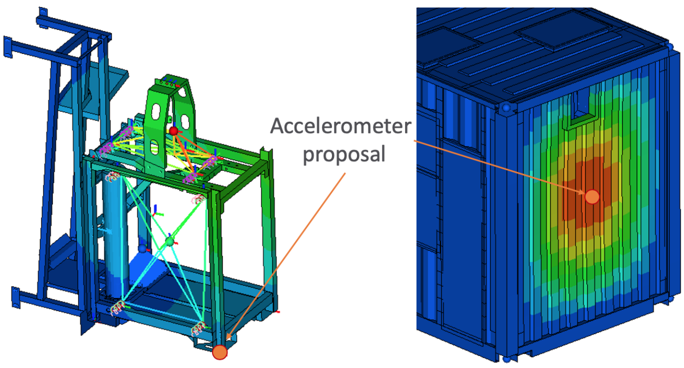

Figure 3.7: *The orange dots shows a proposal of where to place the accelerometers in the direct mobility test. There are isolated modes on the engine frame and at the front wall.*

3.3.2 Frequency Response Measurements

The EMA was performed at Azelio's test plant in Åmål on April 22, 2020. It was sunny weather throughout the day and wind speeds around 2 to 4 m/s. The test plant was not completely shut off. One of the TES units was filled with melted aluminium and pumps were working on the other one. As described in the test plan, the EMA contained three sub-tests: a vibration isolation test, a structural response test and a direct mobility test. All tests were performed with and impact hammer, using the equipment that was specified in Section 3.3.1. The accelerometers were attached using both beeswax and electrical tape.

The toolbox abraDAQ was used for data acquisition in Matlab. Data was gathered in a frequency range from 5 to 300 Hz, using a sample rate of 20 kHz, to be able to catch at least the response for the modes that are of interest when the PCS is operating. Initially, a sample time of 10 s was used but it was lowered to 5 s since it was found that the system is strongly damped. Data from five impacts with the hammer were averaged to reduce noise and get clearer response. The time history and frequency response data from each measurement was saved for doing a state-space identification at a later moment.

The same documentation procedure was used in all sub-tests. The location of excitation and response points were documented in an excel-file after measuring the coordinates from a nearby reference point. Pictures were taken of each test-configuration showing the placement of the accelerometers and their coordinates, that were written on a post-it.

The vibration isolation test began with finding excitation points on the source side of one of the engine mounts. This was done by checking if the excitation point was accessible so that a sufficiently large excitation force could be used. It was difficult to find an excitation point in the x-direction, therefore, only an excitation point in z-direction was used. The location of the point can be seen in Figure 3.8b. However, the response was still measured in both the x- and z-direction by attaching one accelerometer on each side of the engine mount. Pictures of the two configurations can be seen in Figure 3.8. Only one engine mount was tested since it was difficult to access the others.

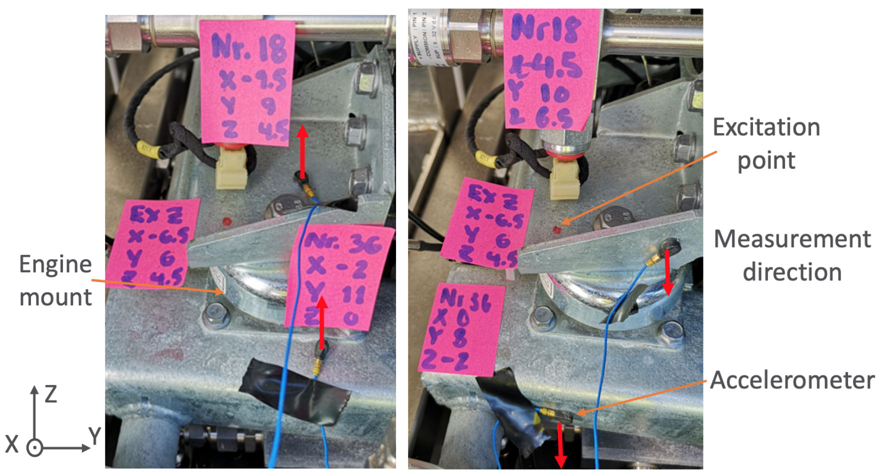

(a) *Response in z-direction* ***(b)*** *Response in x-direction*

Figure 3.8: *Configurations of the vibration isolation test of the engine mounts with an excitation in the z-direction. The red arrows show the direction of the measured response.*

In the structural response test, excitation points were found in both the x- and z-direction in a similar way as in the vibration isolation test. Accessible points on the engine frame where a sufficiently large force could be applied were considered. The excitation points found can be seen in Figure 3.9.

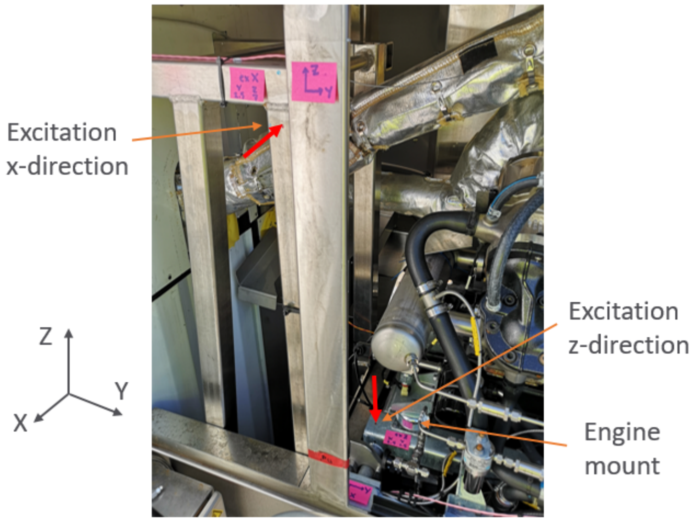

Figure 3.9: *The TES system was excited in the x- and z-direction on the engine frame in the structural response test. The red arrows show the direction of excitation.*

Initially, it was intended to test which location on a part that would give the best response by performing a direct mobility test. However, it was difficult to motivate which point would give the best response when the TES system would be excited at the engine frame instead, so this test was not performed. Therefore, the locations were arbitrarily chosen on the parts that were proposed to be measured in the test plan. Four different configurations of accelerometer placements were tested with the response being measured in a total of nine points, which are shown in Figure 3.10. In all configurations, one accelerometer was placed in point 3 to be able to compare the configurations.

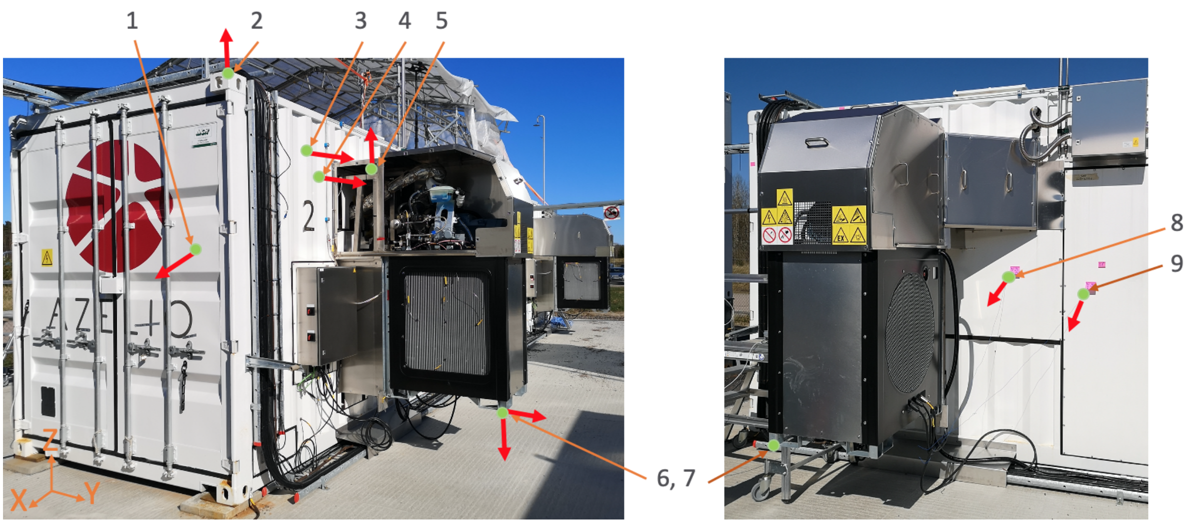

Figure 3.10: *The Figure shows the sensor placement numbers in the structural response test. The response was measured in a total of nine points and the red arrows show in what direction the response was measured in each point.*

One direct mobility test was performed on the engine frame. The sensor was placed in point 7 in Figure 3.10 and the structure was excited 1 cm from the accelerometer, as can be seen in Figure 3.11. In the test plan, it was also suggested to perform a test on the front wall of the container. This test was excluded since there were parts attached to the wall that were not included in the structural FE-model, such as ventilation. Thus, it was uncertain whether the front wall had isolated modes or not.

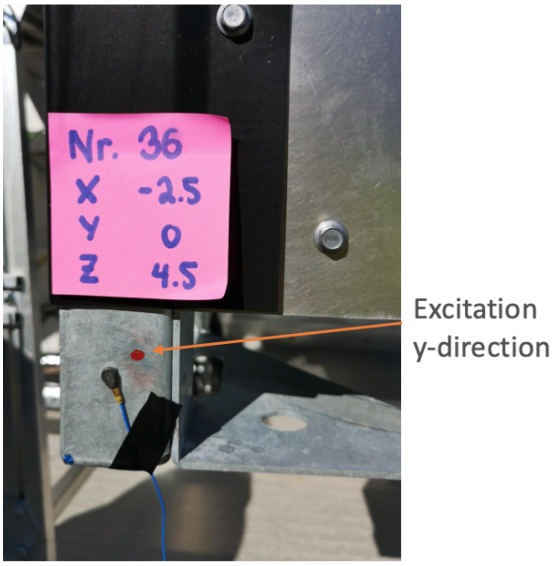

Figure 3.11: *The set-up for the direct mobility test, which was performed at the bottom corner of the engine frame, corresponding to point 5 in Figure 3.10. The TES system was excited in the y-direction, close to the accelerometer.*

3.3.3 Signal Processing

The signal processing was done in Matlab. The test data had already been processed in the sense that the response from the five impacts with the hammer had been averaged in abraDAQ. This reduced the noise and made it easier to distinguish the structural response. The processing was done using data from one of the structural response tests. The configuration that was most representative of how the TES system behaves, had the least amount of noise and most distinct peaks was chosen. This was when the TES system was excited in the x-direction and the response was measured on the panel and the container corner, corresponding to point 2, 3 and 4 in Figure 3.10. The signal from the accelerometer on the container corner was not included in the estimation since this was merely used as a control point.

From the data set, a State-Space Model (SSM) was estimated using the state-space identification toolbox in Matlab. In the estimation, the order of the mathematical model had to be chosen. The order corresponds to half the number of natural frequencies that are captured in the measurement. It can be estimated by the number of peaks that can be identified in the stability chart in Figure 3.12. Moreover, it can be estimated from the curve fitting plot. A model order of 36 was selected for when the red and blue dots in the curve fitting plot have a similar value. The red dots correspond to the Norm of Square Error (NRMSE) and the blue dots corresponds to the Frequency Response Assurance Criterion (FRAC). In addition, this plot displays the correlation between EMA and SSM at a certain order. In this case, the FRAC correlation is about 35 %.

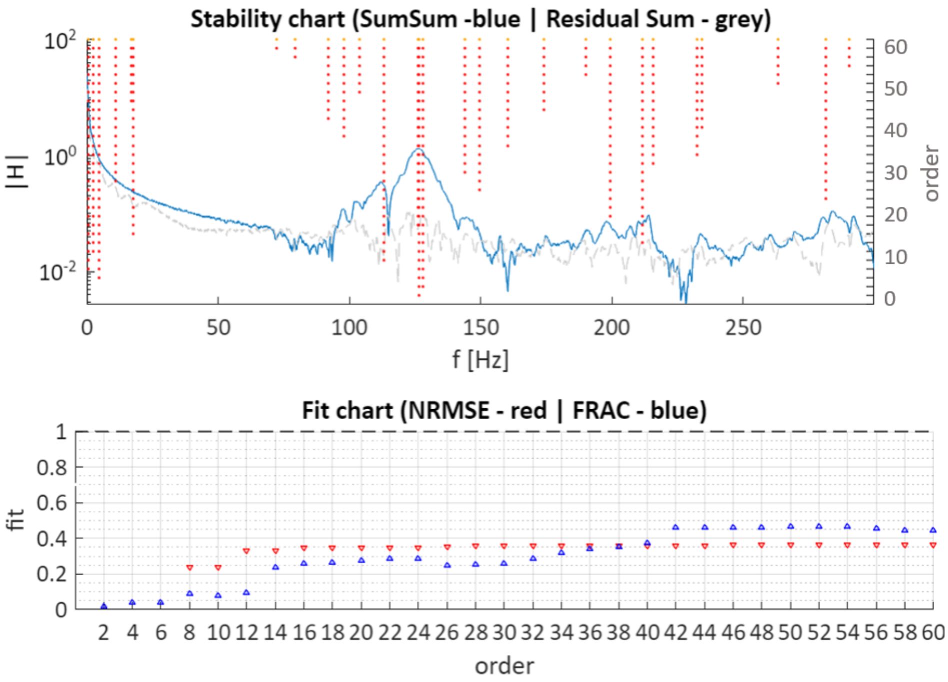

Figure 3.12: *The stability and fit chart from the state-space identification that was done in Matlab.*

After identifying a SSM, the modal damping of each identified mode was computed using the half power bandwidth method, described in Section 2.6. Each part of a structure will have different modal dampings, that can be difficult to obtain for a complex system. Therefore, the assumption that the whole TES system will have a global damping was made. To get a global damping, the modal damping from the SSM had to be averaged between the natural frequencies of 10 to 150 Hz. This span was chosen since frequencies below 10 Hz were considered to be noise and above 150 Hz were out of interest since the highest excitation frequency of the TES system goes to 100 Hz, see Table 1.2. Eight modal dampings could be found between 10 to 150 Hz, seen in Figure 3.13. Looking at the Figure, three values are outliers and were not included in the averaging since they are much bigger than the rest and are considered to be noise response. The averaged damping became 1.63 %. The global damping in the structural FE-model was assigned to this value to be able to compare the FEA with the EMA and the SSM. The global damping of 1.63 % is close to the value Fukuwa, Nishizaka, Yagi *et al.* obtained in their measurements [41]. They executed several tests on a steel-framed building to find out the damping ratio. In the measurements, the damping ratio varied between 1.75 to 3.64 % with a median of 2.2 %.

No further processing of the data from the vibration isolation tests or the direct mobility test was performed. The reason for this will be discussed further in Section 5.2.

3.3.4 Simulated EMA

To be able to compare the results from the EMA and FEA, a harmonic analysis was performed. In the harmonic analysis, the structural FE-model was excited with a unit load in either the x- or z-direction to mimic the excitation in the EMA. A unit load was chosen since the response from EMA is normalized against the load. The response was

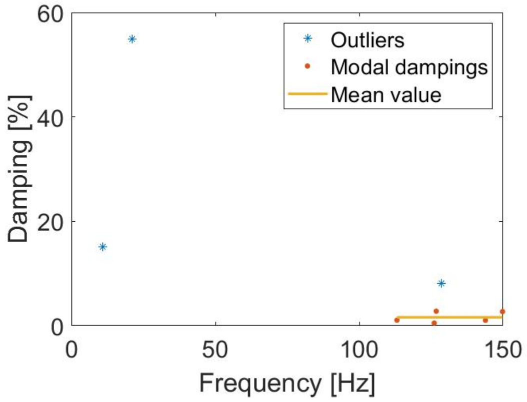

Figure 3.13: *Plot of modal damping values obtained from the SSM. Three values are outliers and were not included for computing the global damping.*

sampled at each frequency up to 150 Hz, which meant that modes had to be solved up to $2.5 \cdot 150 = 375$ Hz in the modal analysis. This happened when 1349 modes were solved. The location of the excitation and response points were close to the locations used in the EMA, see Figure 3.9 and 3.10, respectively. The locations in the structural FE-model was selected on nodes, which positions were constrained by the element size. Therefore, there was a slight difference between the locations in the FEA and EMA.

From the response points, the output was given as the displacement that was written to a text file. The amplitude of the acceleration $\ddot{\hat{q}}_n$ at each frequency f_n could be computed through time differentiating the amplitude of the displacement $\hat{q}_n$ in equation 2.9 in Matlab as

$$\ddot{\hat{q}}_n = (i\omega_n)^2 \hat{q}_n = -(2\pi f_n)^2 \hat{q}_n \quad n = 1, 2, ..., 150 \tag{3.4}$$

to be able to compare the output from the EMA.

3.4 Exterior Acoustics

An acoustic FEA of the exterior sound radiated from the TES system was performed in Ansys Mechanical APDL. Sound radiates from the system due to structural vibrations caused by the Stirling engine. To verify that it is one-way coupling between the structure and fluid so that the surrounding air does not influence the system, the coupling coefficient α was computed using equation (2.26), as

$$\alpha = \frac{c\rho_{fluid}}{2\pi f_{min} d_{mean} \rho_{solid}} = \frac{343.24 \cdot 1.2041}{2 \cdot \pi \cdot 20.83 \cdot 0.003 \cdot 7,800} = 0.13 \tag{3.5}$$

using the properties of air and steel from Table 1.1, the minimum frequency f_{min} seen in Table 1.2 and the average effective thickness of the system d_{mean}, which is about 3 mm. Since α is less than one, the coupling is one-way.

The structural vibrations due to the free mass engine loads were computed in a harmonic analysis of the TES system. The structural vibrations were then used to generate sound waves in an acoustic analysis of the surrounding air, where the sound pressure level in a region around the system was determined. The size of the region, called the acoustic domain, depends on where the sound level should be predicted.

3.4.1 Specification of Domain Size & Sound Level

Azelio has developed a preliminary sound level requirement on the TES system, but it has not yet been established and may change. The requirement is that the noise from one Stirling engine shall not exceed 70 dB at 25 m in a free field at 1.7 m above a flat ground. They have also specified that the noise from the system should be measured according to the international standard ISO 3744:2010. Because of the uncertainties in the internal noise level requirement, the size of the acoustic domain was determined based on ISO 3744:2010. This standard was also used because it gave a shorter distance than 25 m, which saves computational time.

The International Standard ISO 3744:2010 specifies various methods for measuring the A-weighted sound pressure levels of different noise sources, such as machinery [42]. The sound level is measured over a hypothetical measurement surface enclosing the source. The measurement surface can for instance have the shape of a hemisphere, a parallelepiped or a cylinder. The shape depends on the source. For the TES system, a hemisphere with one reflecting plane, representing the ground was chosen. The measurement radius r_{meas} of the hemisphere was computed to be twice as large as the distance from the origin to the farthest corner of the structure d_0

$$d_0 = \sqrt{\left(\frac{l_1}{2}\right)^2 + \left(\frac{l_2}{2}\right)^2 + l_3^2} = \sqrt{\left(\frac{2.42}{2}\right)^2 + \left(\frac{12.18}{2}\right)^2 + 2.87^2} = 6.89 \text{ m} \tag{3.6}$$

$$r_{meas} = 2 \cdot d_0 = 13.78 \text{ m} \tag{3.7}$$

where l_1, l_2 and l_3 are the dimensions of the TES system that can be seen in Figure 3.14a along with d_0.

The measurement points are located 1.5 m and $0.75 \cdot r_{meas} = 10.3$ m above the ground every 45^o, see Figure 3.14b. However, 10.3 m is not of interest since it is mainly the sound during maintenance or surveillance of the TES system that should be predicted.

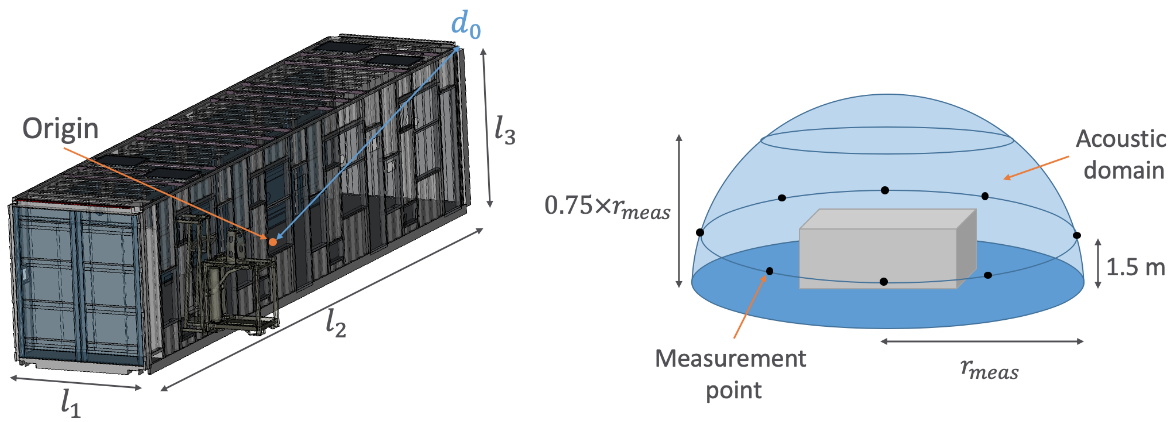

(a) *Dimensions of the TES system* ***(b)*** *Acoustic domain of measurement*

Figure 3.14: *Dimensions of the TES system and the acoustic free field computed from ISO 3744:2010(E) [42].*

ISO 3744:2010 does not specify any requirements regarding sound level. To get an A-weighted sound level requirement, noise regulations from AFS 2005:16 was used. In AFS 2005:16, regulations to noise exposure at work are stated. During daily noise exposure for 8 h, the sound level is allowed to be up to 85 dB(A) [43].

3.4.2 Fluid FE-Model

To solve the exterior acoustics problem, a numerical model of the air surrounding the system had to be created. The air is a fluid domain that can be constructed as a hemisphere volume that encloses the TES system, see Figure 3.14b. This volume was created in Ansa, by first filling bigger openings on the structural FE-model to get a closed volume to be able to do a wrap mesh. By wrapping the TES system, a radiation interface between the fluid and the structure is created. After that, a shell hemisphere was created. The radius of the hemisphere was chosen to be 15.8 m since for this size, the sound can be measured from a distance of $r_{meas} = 13.78$ m, see equation (3.7), without the measurement points being located on the boundary.

To reduce the size of the model, the volume was decreased by making multiple cuts. The hemisphere was cut at 7 m above ground since the radiation above this height is not of interest for evaluating sound levels during maintenance of the operating TES system. Furthermore, only a quarter of the model was analysed by cutting the volume in planes normal to the x- and y-axis where symmetry was assumed, even though the structure is not symmetric. The final acoustic volume can be seen in Figure 3.15.

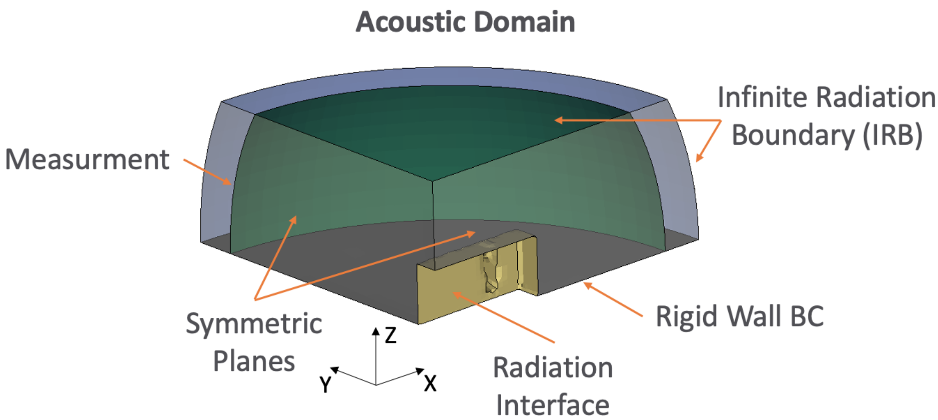

Figure 3.15: *The acoustic domain for which symmetry, rigid wall and absorbing BC were applied.*

The volume was discretized with tetrahedral fluid elements without Fluid-Structure Interaction (FSI). The model consists of 6,000 DOF and 27,000 volume elements. The elements were given the properties of air that are listed in Table 1.1. The element size was chosen with respect to equation (2.21) where the minimum wavelength λ_{min} for a maximum frequency f_{max} of 100 Hz, see Table 1.2, is

$$\lambda_{min} = \frac{c}{f_{max}} = \frac{343.24}{100} \approx 343 \text{ cm} \tag{3.8}$$

For linear fluid elements constructed in Ansys, it is recommended to use twelve elements to resolve the minimum wavelength $N_{e,w}$ [4]. This was used at the interface, $l_{e,in}$, while the outer boundary $l_{e,out}$ had four elements per minimum wavelength.

$$l_{e,in} = \frac{\lambda_{min}}{N_{e,w}} = \frac{343}{12} = 28.6 \text{ cm}, \quad l_{e,out} = \frac{\lambda_{min}}{N_{e,w}} = \frac{343}{4} = 85.6 \text{ cm} \tag{3.9}$$

The element size increased gradually through the domain, from 25 cm at the interface to 75 cm at the outer boundary, to save computational time.

In Section 1.1 it was mentioned that the levelling blocks that are placed on concrete. Therefore, the ground was assumed to reflect sound waves and a rigid wall (Neumann) BC was applied. The outer boundary was modelled to absorb pressure waves since the acoustic domain has to be treated as an infinite exterior boundary [44]. In Ansys Mechanical APDL, there are three ways of modelling a wave-absorbing condition: using an Infinite Radiation Boundary (IRB), Artificially Matched Layers (AML) or Absorbing Boundary Elements (ABE). For IRB, pressure waves that are normal to the boundary are absorbed while waves that strike the boundary at an angle will reflect into the domain [45]. Also, if the radiation boundary is too close to the structure, numerical errors may occur. Therefore, it is more accurate to use AML or ABE since these element types can absorb the wave without any reflection. Both AML and ABE are dependent on the geometry of the enclosure. For AML, elements have to be located inside a cubic or convex enclosure [46], while ABEs have to be located in a spherical enclosure that is centred at the origin [44]. Due to the enclosure restrictions of AML and ABE, IRB was chosen. The boundary is far from the TES system, therefore, no numerical errors should occur.

3.4.3 Structural Harmonic Analysis

A harmonic response analysis was performed using the mode-superposition method on the structural FE-model to compute the structural vibrations that arise due to the free mass loads of the Stirling engine. The mode-superposition method was used since this method is faster to use compared to the full method when performing a harmonic analysis, see Section 2.4.

The TES system was excited with the free mass loads in the point representing the centre point between the main bearings in the Stirling engine, see Figure 1.4. The free mass loads can be found in Appendix A. The frequency domain representation of the free mass loads was given at four discrete engine speeds ranging from 1,250 to 2,000 rpm, for three engine orders. Each load has a different magnitude and phase. To account for the phase offset between loads of different engine orders, they were added on complex form with a real F_{Re} and imaginary F_{Im} part, as

$$F_{Re} = F_0 \cos(\varphi) \qquad F_{Im} = F_0 \sin(\varphi) \tag{3.10}$$

where F_0 represents the magnitude and φ the phase.

The three engine orders were solved separately in three different load steps. The structural response of the four discrete engine speeds was computed at each load step with the frequency ranging from: 20.83 Hz to 33.33 Hz for the first engine order, 41.67 to 66.67 Hz for the second engine order and between 62.5 to 100 Hz for the third engine order. At the engine speed 2,000 rpm, the second and third engine order frequency range overlap. Therefore, the analysis for 2,000 rpm was solved in a separate analysis.

After solving the harmonic analysis, a set of nodes on a fourth of the outer surface of the structural FE-model was selected. It was the same fourth that was modelled in the Fluid FE-model, see Figure 3.15. The accelerations of the selected nodes were written to an asi-file at the discrete engine speeds for each engine order. The asi-file is specifically created to be used in one-way coupling at the interface between the structure and the fluid [47].

To get the total structural response at certain engine speeds, the contribution from each engine order was added in Meta using the superposition principle, see equation 2.11.

3.4.4 Acoustic Analysis

To perform the acoustic exterior analysis, the structural vibration results from the harmonic response analysis were mapped on to the fluid FE-model by reading the asi-file. The structural vibrations were used as a BC at the interface of the fluid. Thereafter, a harmonic acoustic analysis could be performed. The analysis was executed with three load steps in a similar way to the structural one, with the exception that Ansys Mechanical APDL chose the solution method. Therefore, a full harmonic analysis was performed instead of using the mode-superposition method.

The sound pressure in the measurement points seen in Figure 3.16, were of interest. To obtain the result for these, a text file of the pressure at these points was written. The pressure was given for the first, second and third engine order at the discrete engine speeds. From the pressure, the A-weighted sound pressure level could be computed in Matlab using equation (4.4) and by adding the corresponding A-weight at a certain frequency. The total A-weighted sound pressure level was obtained by using equation (2.23).

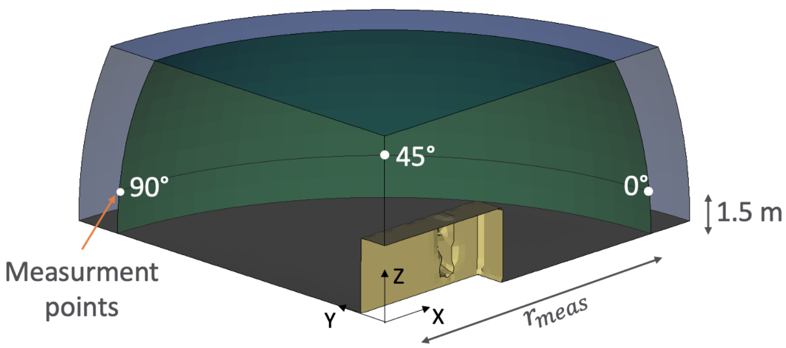

Figure 3.16: *Three different measurement points used for sound evaluation in the far field acoustic domain. The measurement points are obtained by using the method described in ISO 3744:2010(E).*

To get the total sound pressure difference in the acoustic domain at discrete engine speeds, the result from each engine order were used to compute an effective pressure in Meta. The effective pressure was calculated as the RMS-value of the maximum pressure difference p_{max} of each of the three engine orders

$$\tilde{p} = \sqrt{\frac{1}{3}(p^2_{max,eo1} + p^2_{max,eo2} + p^2_{max,eo3})} \tag{3.11}$$

4. Results

In the following sections, the results from the different analyses are presented.

4.1 Modal Finite Element Analysis

In the modal FEA, 897 modes were found in the frequency range up to 250 Hz. The number of modes is plotted versus frequency in Figure 4.1. The curve shows that the number of modes increases with the frequency. The modes shapes are complex in the sense that many parts in the system are moving and not in a clear pattern of moving just in or out of phase. Because of this, no general results from the modal FEA will be presented. Mode shapes from the modal analysis will only be presented in connection with the results of the acoustic analysis.

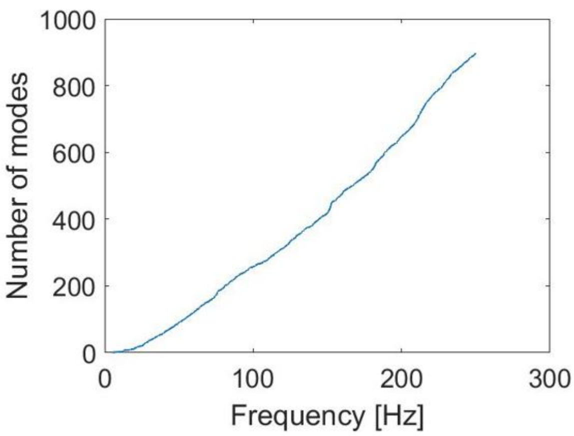

Figure 4.1: *Plot of number of modes versus frequency for the numerical TES system.*

4.2 Structural Response from EMA, SSM & FEA

An EMA was performed, from which a SSM was estimated with data from one of the structural response test configurations. For the chosen configuration, the accelerometers were placed on the container panel, corresponding to point 3 and 4 in Figure 3.10. The excitation was a unit load excited in the x-direction. In Figure 4.2, EMA, SSM and FEA's frequency response functions are shown. In the Figures, it can be seen how the SSM does not catch all of the peaks. The difference between the EMA and SSM is the largest for the lower frequencies. Moreover, the FEA response differs from the EMA and the SSM in both points. The FEA curve is offset to the left in both cases. Furthermore, the magnitude is higher for the EMA and SSM compared to the numerical results, especially at the lower frequencies.

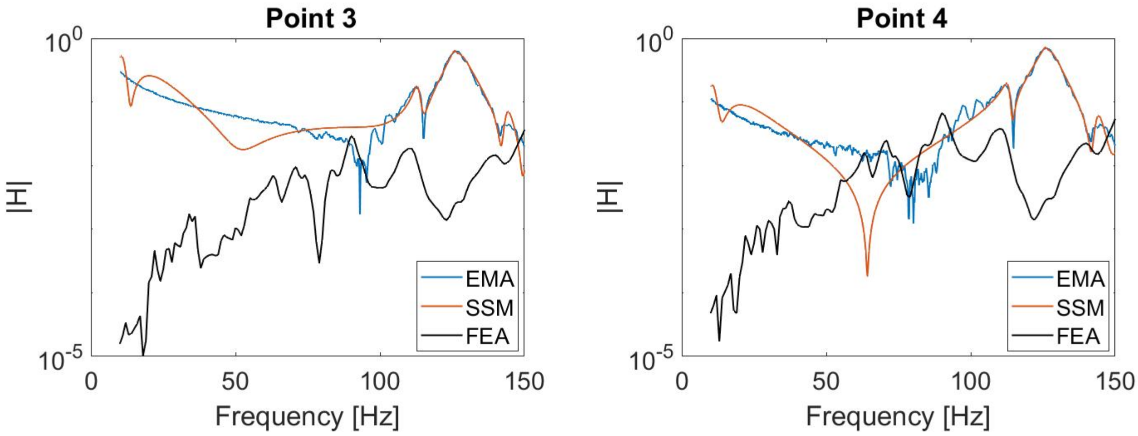

Figure 4.2: *Magnitude of the frequency response functions from EMA, SSM and FEA. The transfer functions are all from a unit-load in the x-direction to response point 3 and 4 located on one of the panels on the container, see Figure 3.10.*

4.3 Acoustic Analysis

The results from the acoustic analysis of the exterior sound radiating from the TES system is presented in this section. The structural vibration results from the harmonic analysis of the TES system and the related exterior sound level results are shown. Lastly, the discretized results at the engine speed where the most sound is radiated are presented. The vibration arises due to the free mass loads. Other parts of the system that can induce vibrations are not included in the results.

4.3.1 Structural Vibrations

The total structural response was computed through the superposition principle at the four discrete engine speeds ranging from 1,250 to 2,000 rpm. The global maximum displacement of all angles at each discrete engine speed can be found in Table 4.1. The maximum displacement near the PCS is displayed at each engine speed in Figure 4.3 and Figure 4.4. At all analysed speeds, the vibrations are concentrated to the engine frame and the area around it. The results show that the system vibrates most at 2,000 rpm out of the speeds. Furthermore, it can be seen in Figure 4.4b that the hatches on the container vibrate more at 2,000 rpm than at the other speeds. At engine speed 1,750 rpm, the engine frame has the most deformation out of the speeds, see Figure 4.4a.

Table 4.1: *Global maximum displacement of the total structural response at each analysed engine speed.*

Engine speed [rpm]	1,250	1,500	1,750	2,000
Maximum displacement [mm]	0.16	0.08	0.26	0.32

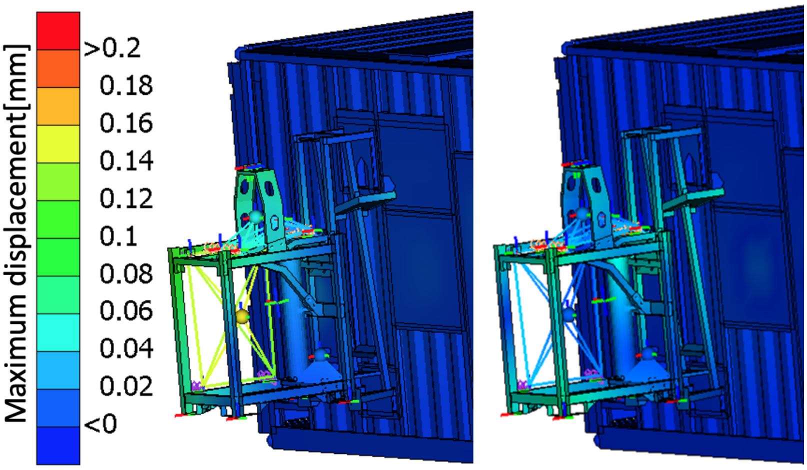

(a) *1,250 rpm* ***(b)*** *1,500 rpm*

Figure 4.3: *The maximum displacement of all angles of the total structural response.*

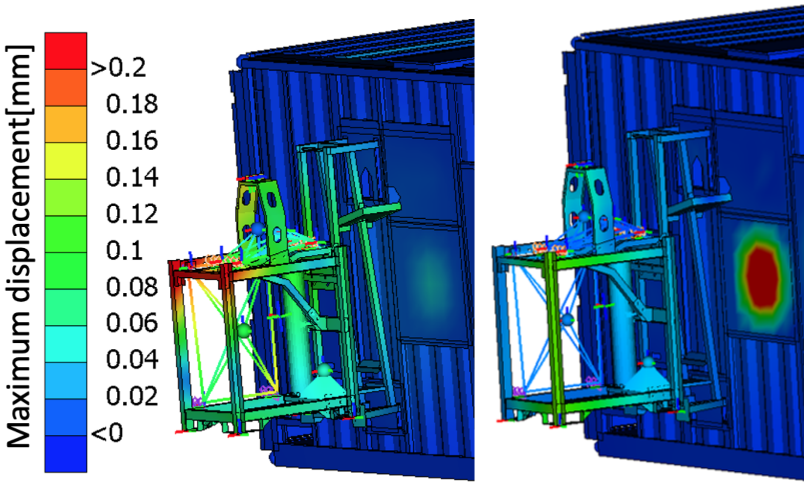

(a) *1,750 rpm* ***(b)*** *2,000 rpm*

Figure 4.4: *The maximum displacement of all angles of the total structural response.*

4.3.2 Exterior Sound

The exterior sound radiates, due to the structural vibrations presented in the previous section. To get the total pressure difference, the effective pressure was computed. The results are shown in Figure 4.5 and Figure 4.6. The figures display a cross section of the acoustic domain 1.5 m above the ground. The contour plot shows the maximum pressure difference from the atmospheric pressure when the Stirling engine is operating between 1,250 and 2,000 rpm. In Table 4.2, the global maximum value at each speed can be found. The pressure difference is greatest when the engine is running at 1,750 and 2,000 rpm and the least at 1,250 and 1,500 rpm. At all analysed speeds, the pressure difference is largest around the engine frame. In the structural results in Figure 4.4b, it can be seen how the hatches to the right of the engine frame vibrate. Comparing the structural results to the corresponding acoustic results in Figure 4.6b, the pressure difference is large to the right of the engine frame where the hatches are located. By comparing the results, the relation between the structure and the fluid can be seen.

Table 4.2: *Global maximum pressure difference of the total acoustic result at the analysed engine speeds.*

Engine speed [rpm]	1,250	1,500	1,750	2,000
Maximum pressure [Pa]	0.73	1.08	2.51	2.31

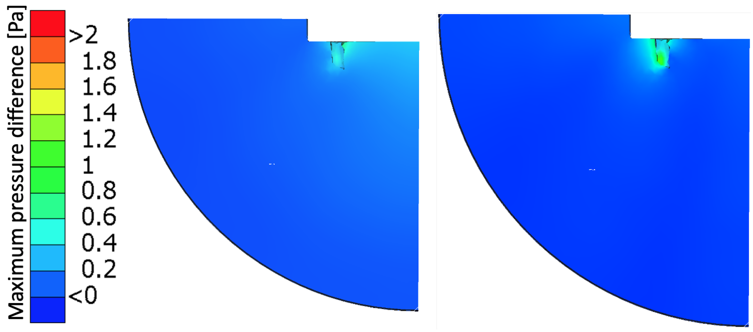

(a) *1,250 rpm* ***(b)*** *1,500 rpm*

Figure 4.5: *A cross section shown from 1.5 m above the ground displaying the maximum pressure difference of all angles from the atmospheric pressure of the acoustic domain.*

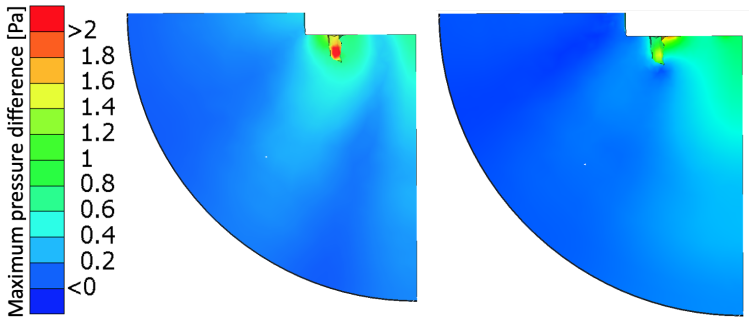

(a) *1,750 rpm* ***(b)*** *2,000 rpm*

Figure 4.6: *A cross section shown from 1.5 m above the ground displaying the maximum pressure difference of all angles from the atmospheric pressure of the acoustic domain.*

In Table 4.3 the total A-weighted sound pressure levels are listed at each engine speed for three points, which location can be found in Figure 3.16. The sound is highest for engine speed 1,750 rpm with 2,000 rpm being slightly lower. The maximum A-weighted sound pressure level is 53.69 dB(A) and is obtained at the measurement point located at 90^o.

Table 4.3: *The total A-weighted sound pressure response for each engine speed calculated in the measurements points seen in Figure 3.16.*

	A-weighted sound pressure level [dB(A)]		
	0^o	45^o	90^o
1,250 rpm	42.36	36.23	27.94
1,500 rpm	40.45	33.16	35.98
1,750 rpm	49.38	53.24	53.69
2,000 rpm	48.71	49.90	46.23

4.3.3 Discretized Results at Engine Speed 1,750 rpm

The results from each engine order when the Stirling engine is operating at 1,750 rpm are presented in this section. The results were discretized at 1,750 rpm since the largest A-weighted sound pressure level was obtained at this speed, see Table 4.3.

The discretized structural response at engine speed 1,750 rpm is shown in Figure 4.7. The maximum displacement is largest for the first engine order, with a value of 0.31 mm. The second and third engine order has a global maximum displacement of 0.13 and 0.005 mm, respectively.

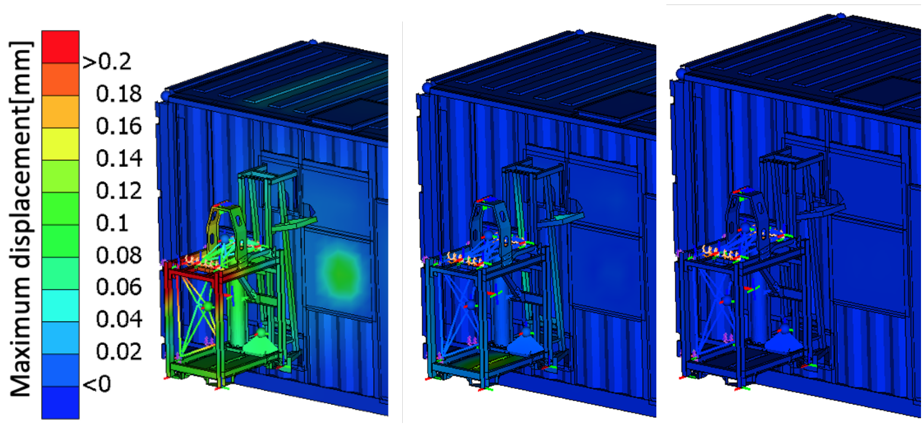

(a) *Order 1* ***(b)*** *Order 2* ***(c)*** *Order 3*

Figure 4.7: *The maximum displacement of all angles at engine speed 1,750 rpm.*

Figure 4.8 shows the maximum pressure difference from the atmospheric pressure of all angles for each engine order when the engine is operating at 1,750 rpm. The global maximum pressure difference is 1.59, 4.29 and 0.18 Pa for the first, second and third engine order, respectively. The pressure difference is largest for the second engine order while the third engine order is much smaller.

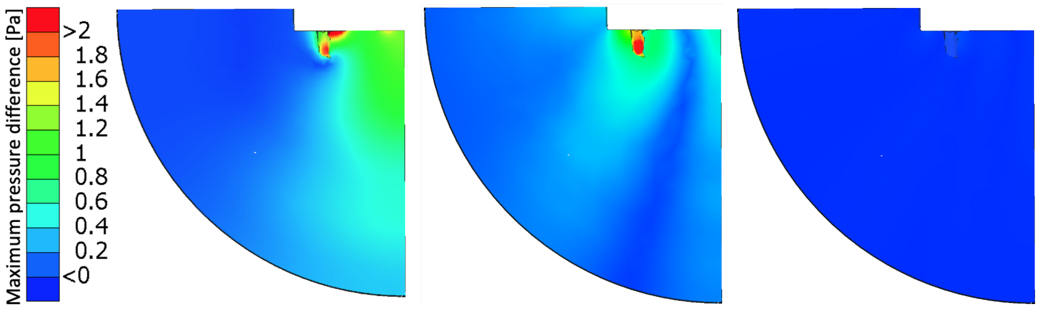

(a) *Order 1* ***(b)*** *Order 2* ***(c)*** *Order 3*

Figure 4.8: *A cross section shown 1.5 m above the ground displaying the maximum pressure difference of all angles from the atmospheric pressure of the acoustic domain.*

The A-weighted sound pressure level at the engine speed 1,750 rpm was calculated for each engine order at the three measurement points. The results are listed in Table 4.4. The location of the points can be seen in Figure 3.16. The sound is highest around 90^o, with the largest contribution coming from engine order two. This can be seen by looking at Figure 4.8b, where the pressure difference is larger at the 90^o point, located along the vertical axis compared to the 0^o point, located along the horizontal axis. Since the sound pressure level is A-weighted, the contribution from engine order three is larger than what would be expected when looking at the pressure difference that can be seen in Figure 4.8c. This is because the frequency is larger for engine order three and, therefore, is in a more sensitive hearing range compared to engine order one and two.

Table 4.4: *The A-weighted sound pressure response at engine speed 1,750 rpm calculated in the measurements points seen in Figure 3.16. The 0^o point is located along the horizontal axis in Figure 4.8, and the angle is measured counterclockwise.*

	A-weighted sound pressure level [dB(A)]		
	0^o	45^o	90^o
Order 1	30.43	19.43	35.61
Order 2	49.26	53.21	53.61
Order 3	31.50	29.59	27.39
Total	49.38	53.24	53.69

Since the highest sound pressure level was identified for the first and second engine order, the modes around the corresponding frequencies were analysed to give information about which modes might be active in the harmonic analysis. These are called critical modes. Table 4.5 and 4.6 presents all identified modes near 29.2 and 58.3 Hz, which corresponds to the first and second engine order at 1,750 rpm. Modes that were 2 Hz above and below 29.2 and 58.3 Hz were studied. For the first engine order, ten modes were found in this frequency range while 14 modes were found at the second engine order. The mode shapes of the TES system are complex and hard to describe. Therefore, the tables in which the modes are presented only contains information about the parts that move the most. Some modes are defined as global since nearly all parts are moving, none more than the other.

Table 4.5: *Identified modes near 29.2 Hz, corresponding to engine order one at engine speed 1,750 rpm. The mode shapes are complex and thus no simple description of these can be given. For this reason are only the moving parts that were identified specified.*

Mode	**Frequency [Hz]**	**Moving Parts**
29	27.50	Roof (rear)
30	27.96	Roof (rear)
31	28.04	Rear doors
32	29.11	Global mode
33	29.42	Engine frame, side doors, roof, hatches
34	29.51	Engine frame, side doors, roof
35	29.60	Engine frame, side doors, roof, hatches (see Figure 4.10)
36	30.04	Side doors, roof, hatches
37	30.20	Side doors, roof, hatches
38	30.77	Global mode (middle)

Table 4.6: *Identified modes near 58.3 Hz, corresponding to engine order two at 1,750 rpm.*

Mode	Frequency [Hz]	Moving Parts
109	56.49	Global mode (middle)
110	56.98	Right wall, roof
111	57.21	Roof (rear)
112	57.35	Roof and hatches (middle)
113	57.55	Roof (front)
114	57.60	Roof (front)
115	58.16	Roof (front)
116	58.49	Engine frame
117	59.03	Global mode (middle)
118	59.41	Global mode (front)
119	59.61	Roof and hatches (front)
120	59.80	Roof, hatches and engine frame (see Figure 4.12a)
121	60.15	Bottom plate engine frame (see Figure 4.12b)
122	60.24	Roof and engine frame

By looking at the modal results, critical modes can be found. Mode number 35 at 29.6 Hz was the one that looked most similar to the first order's structural response at 1,750 rpm, seen in Figure 4.9. Mode 35 is presented in Figure 4.10.

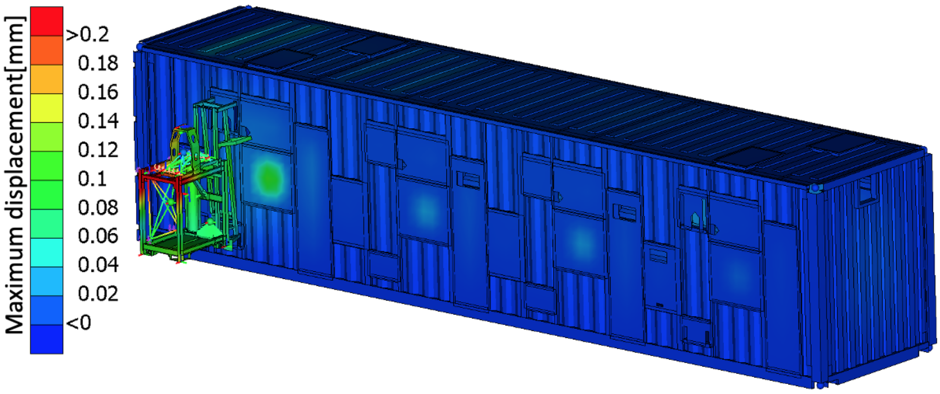

Figure 4.9: *Harmonic response for engine order one at 1,750 rpm.*

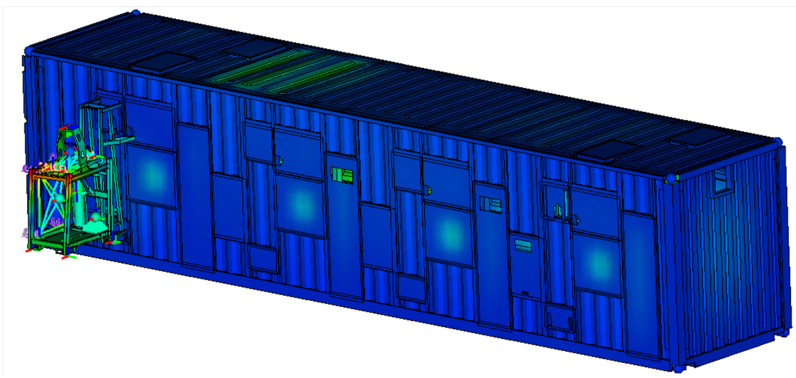

Figure 4.10: *Critical mode at engine order one at 1,750 rpm. The figure displays mode 35 with the natural frequency 29.6 Hz.*

For the second engine order, the most similar modes to the structural response seen in Figure 4.11 was mode number 120 and 121 at 59.8 and 60.2 Hz, respectively. The mode shapes can be seen in Figure 4.12. There could be more critical modes for engine order one and two. The ones that are displayed are just a proposal of which modes that are active at these frequencies. It is mainly these three modes that design changes should be based on to lower the exterior sound level at 1,750 rpm.

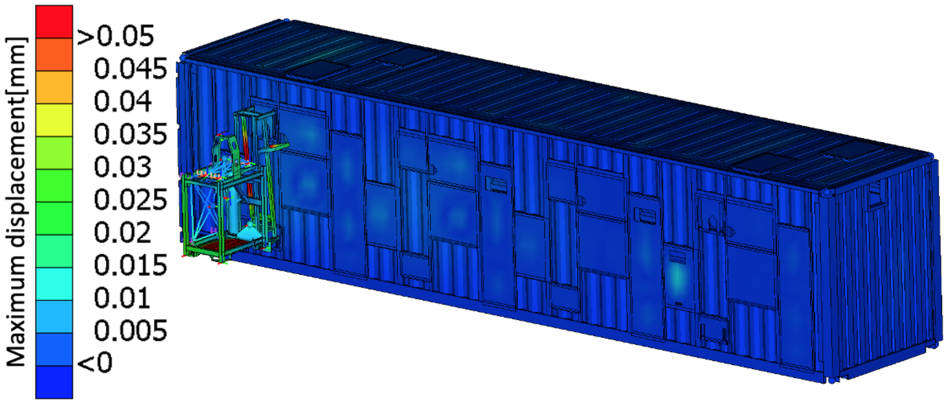

Figure 4.11: *Harmonic response for engine order two at 1,750 rpm.*

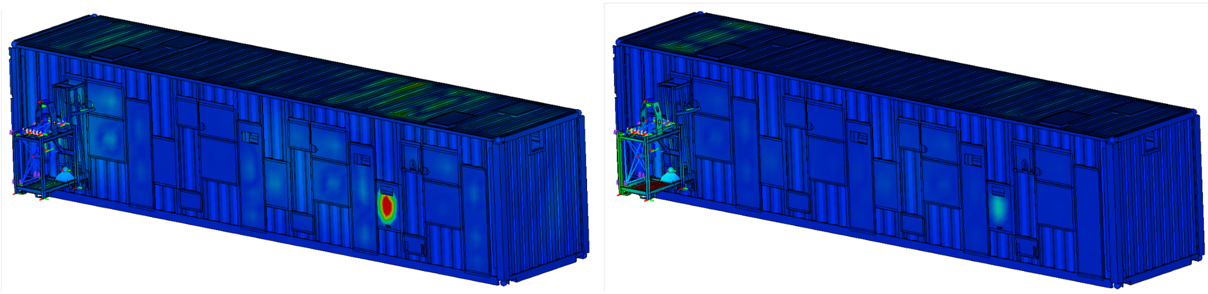

(a) *Mode 120 at 59.8 Hz* ***(b)*** *Mode 121 at 60.2 Hz*

Figure 4.12: *Critical modes at engine order two at 1,750 rpm.*

5. Discussion

In this chapter, a discussion regarding how well the aim is fulfilled is presented together with an evaluation of the results and the method.

5.1 Structural FE-model

The structural FE-model is a simplification of reality, which means that some of the physics is lost. For instance, the TES system was assumed to be linear, but in reality, all systems are non-linear. The simplifications were made to save computational time and to reduce the complexity of the model. The model is still complex considering that 897 modes were found in the frequency range up to 250 Hz.

One simplification made was that some parts were excluded from the model. To account for the missing parts on the PCS, the density of the engine frame was adjusted to get the correct mass, which may affect the stiffness. To account for the mass of other parts, mass elements were used. These were attached with beams, which might not be a realistic representation of how these components are attached to the TES system. That, together with the moment of inertia not being modelled for the mass elements, can have contributed to errors in the result. Furthermore, no information was obtained regarding how the vibration shape of these parts look like since they were assumed to act as rigid bodies.

Beams were also used to model screws and screw holes. Some parts were connected using a bonded contact to simplify the model. The bonded contact is a more realistic representation of parts that have been welded together compared to screwed together. The hatches were also connected using a bonded contact since it is difficult to get a correct representation of these. In reality they are connected with rubber strips and screws.

Several parts had a changed geometry to enable a larger element size. Thus, some information regarding the geometry and how it behaves was lost. The chosen element size was computed to be able to capture the minimum wavelength accurately in the harmonic analysis, but it did not account for the maximum frequency being higher in the simulated EMA. This might not have affected the results for the simulated EMA, but a mesh convergence study could have assured this.

A global damping was assigned to the TES system, even though each part of a structure will have individual damping at each natural frequency. The damping of the engine mounts was modelled as a viscous damper with a damping ratio that was estimated from rubber with similar shore-A hardness. The damping of the engine mounts depends on the frequency. However, the viscous damping was computed from the mean frequency of 60.4 Hz. This means that the damping will be most accurate at frequencies close to this value and less at 20.83 or 100 Hz.

The simplifications and modifications of the structural FE-model can have affected the results in the sense that some modes might not have been captured or were found at the wrong frequency.

5.2 Test Method of EMA

There are several aspects of the test plan and method of the EMA that can be discussed. Preparations were done before the EMA test. Still, it may be possible that the accuracy of the experimental measurement has been compromised due to the methodology and equipment not being ideal. The measurement was planned to be executed earlier to be able to calibrate the FEA against the EMA. However, due to the delayed test, there was no time to calibrate. This resulted in the test data and the chosen measurement points being inadequate for comparison with the FEA. The test plan should, therefore, have been modified for the new time plan and other measurement points should have been chosen. Despite the flaws, the test plan made the EMA more organized and efficient.

The excitation method that was chosen, suited the purpose and conditions of the experiment. Due to the time-limitation, a quick method was important so that many tests and different configurations could be performed in one day. The disadvantage of the method is that the impact force exerted to the structure is limited by the load cell and the size of the hammer. Considering the size of the TES system, it would have been better to use a larger one, but no such was available.

Another factor that can have influenced the results is the other activities that occurred during the day. However, the activities were not close to where the measurements took place and they did not cause much vibration. If they affected the result, the influence could have been reduced by the response being averaged from several impacts with the hammer. The response was averaged to decrease the noise in the signals. However, the averaging is affected by the difference between the impacts with the hammer. For instance, when it comes to striking the hammer at the same point, with a straight angle and without hitting the structure twice.

In the measurement, the accelerometers may not have been properly attached in all tests, since the beeswax did not stick to the surface and the attachment had to be complemented with electrical tape. Furthermore, due to the limited number of channels in the DAQ system, the response could only be measured in three points at a time. Thereby, the SSM will not be representative of the whole TES system. The optimal placement of the accelerometers could have been determined prior to the structural response test using a sensor placement method, to correctly observe the behaviour of the TES system. By not doing that, there is a risk that the accelerometers were placed at nodes of modes, in which the behaviour of the TES system cannot be seen. The placement of the accelerometers could also have been determined by simulating the structural response test before the actual test. Thereby, the results from the EMA and FEA could have been compared directly at the test day and changes in the methodology could instantly have been made depending on the results.

Another deficiency in the structural response test is that the response was measured on components whose mounting is difficult to model. The response was, for instance, measured on hatches attached to the container with rubber frames and bolts, corresponding to point 8 and 9 in Figure 3.10. The response data from the accelerometers that were placed on these components was impractical for comparing the EMA to the FEA. Instead, more points on panels should have been selected.

How the properties of the engine mounts during operation were to be determined from the vibration isolation test was not established prior to the test. When processing the results, it was found that no relevant information could be extracted from the data, since the properties of the engine mounts are frequency dependent. Moreover, the engine mount that was tested was not isolated, which means that the receiver response may have been influenced by vibrations passing through the other mounts. To determine the vibration isolation properties through measurements, the engine must be running and the mount must be isolated.

One direct mobility test was executed without any clear result. Since the test was delayed and the time was limited, the main focus was on determining a global damping of the TES system, not determining the damping of specific parts. Furthermore, it was difficult to evaluate if the tested system had isolated modes or if they only appeared in the modal FEA as a consequence of the parts that were excluded in the model, such as the ventilation at the front wall. Therefore, no data from the direct mobility test was processed.

5.3 Evaluation of SSM

A SSM was created from one EMA configuration when the accelerometers were attached to one of the panels on the TES system, corresponding to point 3 and 4 in Figure 3.10. Looking at Figure 4.2, it can be seen that SSM has not caught all of the measured peaks, which might be noise or the structural response that it has missed. Compliance is especially lacking up to 100 Hz. The inability to capture the behaviour of the panel is also confirmed by the fit chart in Figure 3.12, showing that the correlation between the EMA and SSM is 35 % for order 36. The fit would not improve by choosing a higher order, because more noise would then have been captured by the SSM.

The SSM cannot be said to be representative for the TES system since only two points were used to estimate the SSM. Therefore, the global damping of 1.63 %, that was computed from five modal dampings of the SSM, is questionable. Furthermore, all modal dampings were found at frequencies above 100 Hz and might not be representative of the behaviour below 100 Hz that is of interest. On the other hand, the global damping is similar but slightly lower, than the ones that Fukuwa, Nishizaka, Yagi *et al.* obtained in their measurements of a steel-framed building. Therefore, the global damping is at a reasonable level for this kind of structure.

5.4 Comparison between EMA and FEA

From Figure 4.2 it can be seen that the correlation between EMA and FEA at point 3 and 4, found in Figure 3.10, is lacking, especially at lower frequencies when it comes to the amount of mobility and detected peaks. This is odd considering results from a measurement and a numerical model will usually be the most similar at low frequencies.

In the EMA, there is a low frequency mode that is not detected in the FEA. This could have to do with a tank filled with cooling liquid at the PCS that has not been modelled. As the system vibrates, a wave will propagate in the tank that might affect the system at lower frequencies.

The TES system is rather complex, so it will be difficult to get the models to agree. Neither EMA nor FEA can be considered to capture the true behaviour of the system and it is unsure which one is more correct. Both EMA and FEA consists of multiple imperfections, assumptions and simplifications that can have impacted the results. These have been discussed in Section 5.1 and 5.2. Due to the large differences, the results were not calibrated to look more similar since a calibration cannot compensate for missing physics. For similar results, tuning different parameters could have aligned the curves.

5.5 Acoustics

The following sections discuss the numerical method, the requirements that were used and the results that were obtained from the fluid FE-model.

5.5.1 Specifications

To determine the sound level and domain size, a combination of ISO 3744:2010(E) and AFS 2005:16 was used. Azelio's internal sound requirement was not used since the acoustic domain would be larger, thus the computational time to solve the acoustic problem would be longer.

ISO 3744:2010(E) contains information about where to measure sound, but it does not claim an allowed sound pressure level. As for AFS 2005:16, it is the opposite way. AFS 2005:16 only states a condition for the sound pressure level during daily noise exposure for 8 h at work. A combination of these are not optimal since a person that is servicing the TES system will probably not be at a distance of 13.78 m from the origin. However, if the distance would have been smaller, the far field domain would not be present. Thus, it would be more difficult to measure the sound pressure level since the same assumptions do not apply for near field as for far field. Furthermore, AFS 2005:16 is targeted to daily noise exposure during work. When servicing the TES system, noise exposure will not be daily. Therefore, the sound requirement might be too low for the problem statement.

5.5.2 Numerical Method

FEM was chosen to solve the acoustic problem since this is the solution method used in Ansys Mechanical APDL. The advantages of using this software for the acoustic analysis is that all analyses could be performed in the same program. Thereby, the risk of losing information when transferring data from one software to another was avoided. Furthermore, Ansys Mechanical APDL is a batch code based software, which means that it is easy to repeat the analysis using other geometries or loads. The company wants a generic method that can be used to evaluate different designs and for that, Ansys Mechanical APDL is very useful.

The disadvantage of using a FEM solver is that it is not ideal to analyse exterior far field sound from a structure of this size. Due to the size of the computational domain, it is more beneficial to use software that has implemented either BEM or WBT. However, if near field sound or interior acoustics is assessed for working environment requirements, the FEM based solution might have a lower computational cost compared to the other methods.

5.5.3 Fluid FE-model

The fluid FE-model consists of a hemisphere that surrounds the TES system. To reduce computational time, the fluid domain size was reduced. It was reduced by cutting the hemisphere 7 m above the ground and creating symmetry at planes normal to the x- and y-direction so only a fourth of the model was evaluated. However, the TES system is not symmetric, so this simplification is not accurate. Furthermore, four elements per minimum wavelength were used at the outer domain. This might affect the accuracy of the results since twelve elements per minimum wavelength are recommended to use.

To model an absorbing BC at the outer boundary, either ABE or AML are recommended. These were not applied at the outer boundary due to the enclosure restriction of these element types. Therefore, IRB was used instead that can reflect some of the sound waves into the domain. This, however, was not detected when looking at the results.

For the chosen measurement points, seen in Figure 3.16, it was assumed that it was far field. However, in Section 2.8.1 it is stated that far field is entered at a distance of two wavelengths 2λ from the sound source. At the minimum frequency $f_{min} = 20.83$ Hz, see Table 1.2, this would mean that the far field segment l_f enters at a distance of

$$l_f = 2\lambda = \frac{2c}{f_{min}} = \frac{2 \cdot 343.24}{20.83} = 33.96\ m \tag{5.1}$$

when the sound travels through air c. This domain size was not chosen due to the computational time and since the measurement distance computed from ISO 3744:2010(E) is valid from a distance of 13.78 m. However, the far field assumption might not be correct.

5.5.4 Results

The acoustic results themselves are not of interest, but rather the method for interpreting them and how they can be used to evaluate the developed method. The following paragraphs aim to do that.

From Figure 4.8, it can be seen that the first and second order loads from the Stirling engine, when it is operating at 1,750 rpm, gives most contribution to the pressure difference. At the corresponding frequencies, ten and 14 modes were detected in the modal analysis. It is difficult to distinguish from these which ones are critical in the structural harmonic analysis. Figure 4.10 and 4.12 is an attempt to show which modes that might be the most critical. By identifying critical modes, design changes can be made to be able to avoid these.

It was assumed that higher orders loads were negligible since their magnitudes were much smaller than the first three orders. However, if higher orders for the free mass engine loads would have been included, they might have contributed to the A-weighted sound pressure level. A-weighting accounts for how the human ear will respond to sound, see Figure 2.7. Humans are more sensitive to sounds that are higher in the frequency range. Therefore, higher order loads would be in a more sensitive hearing range.

In Table 4.4, the A-weighted sound pressure level at three measurement points are listed. The location of the measurement points can be seen in Figure 3.16. The total response is as most 53.69 dB(A) when the measurement point is located at 90^o. This is less than 85 dB(A), which is a regulation stated by AFS 2005:16 of what is allowed to work in for daily noise exposure during 8 h. However, only the sound induced by the free mass loads from the Stirling engine is included in this calculation and there are probably more parts of the TES system that will make sound radiate. Therefore, the A-weighted sound pressure level is expected to be slightly higher. The sound pressure level could also be low in this frequency range since it is A-weighted. The low A-weighted sound pressure level means that for the current system, no actions need to take place regarding design changes or working with earmuffs.

However, if sound reductions were to be made, it is recommended to run the Stirling engine at 1,250 or 1,500 rpm. At these engine speeds, the least pressure difference could be detected, see Figure 4.5. It is seen in Figure 4.7 that the PCS causes most of the vibrations. This was expected since the loads are excited from there. By, for instance, constructing a new attachment to the container, the amount of vibrations can be reduced and thus also the sound that radiates from the system. When using the developed generic method, the engine speed and parts of the TES system that vibrates much should be evaluated to be able to give recommendations on how to reduce the sound level.

6. Conclusion

The aim was to develop a generic method to simulate the exterior sound radiation from a vibrating system and compare the numerical model with measured test data. The method was created for the TES system when vibrations arise from free mass loads induced by one Stirling engine, but can be applied to similar systems.

Many simplifications were made to get more computational efficient FE-models of the fluid and the structure. These have probably affected the results. However, the goal was to develop a method and not necessarily having the most accurate model.

One measurement was performed and it can only be compared with some of the results from the numerical method. Therefore, the accuracy of the numerical method cannot be verified. The performed measurement was an EMA and the results differ from the FEA. This does not necessarily mean that the developed method is inadequate since the test was performed on a rather complex system.

Overall the aim was fulfilled, it can be seen from the results that the exterior sound pressure level can be obtained at a plane, or in a point, at various engine speeds. The sound level in a point can be compared to measurements, while the plane contour plot can be used in the development process to identify parts that radiate a lot of sound. In the acoustic analysis, a fluid domain was created, in which the structural vibrations at the interface of the domain was used to compute the sound. The structural vibrations were obtained from the mode-superposition harmonic analysis and mapped onto the fluid domain. This approach is general so other designs and loads can be evaluated with this method as well.

6.1 Future Work

From the conclusion, several steps that can be done to improve the method and results.

When evaluating the exterior acoustics in the design process, a definite requirement should be established regarding the allowed maximum sound pressure level and how it should be measured. From this, the size of the acoustic domain can be decided and whether the measurement will take place in the near field or far field. Depending on the field, different assumptions are used. If the size of the acoustic domain is large, another software which uses BEM or WBT should be used instead to reduce the computational time.

To get better results for the current TES system, another EMA should be performed to get more reliable results. In the new measurement, the placement of the actuators should be evaluated so the result can be compared with the FEA. If the results between the EMA and FEA do not coincide, the structural FE-model should be calibrated against the measurement. If the differences are so large that a calibration is impossible to perform, the simplifications that have been made in the structural FE-model should be evaluated to find a balance between accuracy and efficiency. Furthermore, the characteristics of the engine mounts should be examined so that they can be modelled more accurately in the structural FE-model. Lastly, higher orders of the free mass load should be included to see how they would impact the results.

To verify the developed generic method, additional measurements are needed. These measurements should be performed on a simpler system to reduce the number of uncertainties in the results. The measurements should be comparable with the steps that are performed in the numerical method. Such as, getting more information regarding the simpler systems eigenmodes, eigenfrequencies and its vibrating behaviour during loading. Furthermore, a sound measurement should take place where microphones will be located in the same points used in the simulation. If the sound pressure level is similar between the measurement and the numerical model, the numerical method can be used to be able to evaluate different designs when it comes to the exterior sound pressure level.

References

[1] Azelio. (n.d.). Thermal energy storage, [Online]. Available: https://www.azelio.com/technology/thermal-energy-storage/ (visited on 19/03/2020).

[2] Material Property Data. (n.d.). Astm a656 steel, grade 7, [Online]. Available: http://www.matweb.com/search/datasheet.aspx?matguid=c75671219abf49428-b7322916afd1c12 (visited on 12/03/2020).

[3] The Wood Database. (n.d.). Keruing, [Online]. Available: https://www.wood-database.com/keruing/ (visited on 12/03/2020).

[4] C. Howard and B. Cazzolato, *Acoustic Analyses Using Matlab and Ansys*. 6000 Broken Sound Parkway: CRC Press, 2015, ISBN: 978-1-4822-2327-9.

[5] E. Ponte. (20th Sep. 2017). Shore hardness and soft tpes, Teknor Apex, [Online]. Available: https://www.teknorapex.com/thermoplastic-elastomers-and-measuring-shore-hardness-chart (visited on 13/05/2020).

[6] K. M. Bataineh, "Numerical thermodynamic model of alpha-type stirling engine", *Case studies in thermal engineering*, vol. 12, pp. 104–116, 2018. DOI: 10.1016/j.csite.2018.03.010.

[7] T. Abrahamsson, *Structural Dynamics and Linear Systems - Compute, Test, Calibrate and Validate*. Chalmers University of Technology, 3rd Nov. 2019.

[8] Ansys. (n.d.). Modal analysis, [Online]. Available: https://ansyshelp.ansys.com/account/secured?returnurl=/Views/Secured/corp/v192/ans_thry/thy_anproc3.html%5C%23anpassumpres (visited on 16/03/2020).

[9] M. Paz and Y. H. Kim, *Structural Dynamics: Theory and Computation*, 6th ed. Gewerbestrasse 11: Springer, 2018, ISBN: 978-3-319-94743-3.

[10] J. Humar, *Dynamics of Structures*, 3rd ed. 6000 Broken Sound Parkway: CRC Press LLC, 2012. [Online]. Available: https://link.springer.com/content/pdf/10.1007/978-3-319-94743-3.pdf (visited on 18/03/2020).

[11] Ansys. (n.d.). Three solution methods for harmonic analysis, [Online]. Available: https://ansyshelp.ansys.com/account/secured?returnurl=/Views/Secured/corp/v201/en/ans_str/Hlp_G_STR4_4.html (visited on 25/05/2020).

[12] ——, (n.d.). Mod-superposition method, [Online]. Available: https://ansyshelp.ansys.com/account/secured?returnurl=/Views/Secured/corp/v192/ans_thry/thy_tool9.html (visited on 18/03/2020).

[13] J. Kocbach, "Finite element modeling of ultrasonic piezoelectric transducers", University of Bergen, Department of Physics, Tech. Rep., Sep. 2000.

[14] Comsol. (19th Apr. 2018). Mode superposition, [Online]. Available: https://www.comsol.com/multiphysics/mode-superposition (visited on 18/03/2020).

[15] H. Bodén, U. Carlsson, R. Glav, H. Wallin and M. Åbom, *Ljud & Vibrationer*. Norstedts Tryckeri AB, 2001, ISBN: 91-7170-434-5.

[16] O. Døssing, "Structural testing part 1, mechanical mobility measurements", Tech. Rep., 1988.
[17] Siemens. (29th Sep. 2019). What is a frequency response function (frf)?, [Online]. Available: https://community.sw.siemens.com/s/article/what-is-a-frequency-response-function-frf (visited on 17/03/2020).
[18] H. Mevada and D. Patel, "Experimental determination of structural damping of different materials", *Procedia Engineering*, vol. 144, pp. 110–115, May 2016.
[19] Massachusetts Institute of Technology. (2005). Second-order systems, [Online]. Available: https://ocw.mit.edu/courses/mechanical-engineering/2-003-modeling-dynamics-and-control-i-spring-2005/readings/notesinstalment2.pdf (visited on 26/03/2020).
[20] P. Avitabile, "Experimental modal analysis", *Sound and Vibration*, vol. 35, no. 1, 2001.
[21] J. Zhao, "Experimental modal analysis overview", *Crystal Instruments*, no. 43, Apr. 2017.
[22] A. Cunha and E. Caetano, "Experimental modal analysis of civil engineering structures", *Sound and Vibration*, 2006. [Online]. Available: https://repositorio-aberto.up.pt/bitstream/10216/67103/2/56957.pdf (visited on 30/04/2020).
[23] Comsol. (11th Jun. 2018). Introduction to acoustics, [Online]. Available: https://www.comsol.com/multiphysics/acoustics (visited on 18/03/2020).
[24] Siemens. (29th Aug. 2019). Near Field versus Far Field, [Online]. Available: https://community.sw.siemens.com/s/article/sound-fields-free-versus-diffuse-field-near-versus-far-field (visited on 11/05/2020).
[25] Science Direct. (n.d.). A-weighting, [Online]. Available: https://www-sciencedirect-com.proxy.lib.chalmers.se/topics/engineering/a-weighting (visited on 25/03/2020).
[26] R. A. Dobie and S. Van Hemel, "Basics of sound, the ear, and hearing", in *Hearing Loss: Determining Eligibility for Social Security Benefits*, National Academies Press, 2004, ISBN: 0-309-54514-5.
[27] P. P. Urone and R. Hinrichs, "Speed of sound, frequency, and wavelength", in *Collage Physics*, M. J. Crocker, Ed., Rice University, 2019, ch. 17.2.
[28] Nti Audio. (n.d.). Frequency-weightings for sound level measurements, [Online]. Available: https://www.nti-audio.com/en/support/know-how/frequency-weightings-for-sound-level-measurements (visited on 20/03/2020).
[29] O. Runborg, "Helmholtz equation and high frequency approximations", KTH Computer Science and Communication, Tech. Rep. DN2255 – Numerical Solutions of Differential Equations, Lecture Notes 5, 2012.
[30] S. Kirkup and J. Yazdani, "A gentle introduction to the boundary element method in matlab/freemat", East Lancashire Institute of Higher Education, Tech. Rep. AR-08-14, 2008.
[31] H. Antes, "A short course on boundary element methods", Technische Universität Braunschweig, Tech. Rep., 2010.
[32] B. Pluymers, W. Desmet, D. Vandepitte and P. Sas, "Application of an efficient wave-based prediction technique for the analysis of vibro-acoustic radiation problems", *Journal of computational and applied mathematics*, vol. 168, no. 1-2, pp. 353–364, 2004. DOI: 10.1016/j.cam.2003.05.020.
[33] Ansys. (n.d.). One-way coupling from single physics to acoustics, [Online]. Available: https://ansyshelp.ansys.com/account/secured?returnurl=/Views/

Secured/corp/v201/en/ans_acous/acous_adv_unicou.html?q=one-way%5C%20coupling (visited on 27/04/2020).
[34] F.-K. Benra, H. J. Dohmen, J. Pei, S. Schuster and B. Wan, "A comparison of one-way and two-way coupling methods for numerical analysis of fluid-structure interactions", *Journal of applied mathematics*, vol. 2011, 2011. DOI: 10.1155/2011/853560.
[35] Ansys. (6th Jul. 2009). Acoustic applications in mechanical engineering, Ansys, [Online]. Available: https://www.nti-audio.com/en/support/know-how/frequency-weightings-for-sound-level-measurements (visited on 20/03/2020).
[36] A. Schiavi and A. Prato, "Elastic and viscoelastic properties of synthetic rubber (polychloroprene): Dynamic and static characterization", Proceedings of the 24nd International Congress of Sound and Vibration (ICSV), Tech. Rep., Jul. 2017.
[37] Neos Guide. (2019). Augmented lagrangian methods, [Online]. Available: https://neos-guide.org/content/augmented-lagrangian-methods (visited on 15/05/2020).
[38] Ansys. (n.d.). Eigenvalue and eigenvector extraction, [Online]. Available: https://ansyshelp.ansys.com/account/secured?returnurl=/Views/Secured/corp/v192/ans_thry/thy_tool13.html (visited on 30/03/2020).
[39] ——, (n.d.). Comparing mode-extraction methods, [Online]. Available: https://ansyshelp.ansys.com/account/secured?returnurl=/Views/Secured/corp/v192/ans_str/Hlp_G_STR3_15.html (visited on 30/03/2020).
[40] P. Hynnä, "Mechanical mobility technique", VTT Technical Research Centre of Finland, Tech. Rep., Nov. 2002.
[41] N. Fukuwa, R. Nishizaka, S. Yagi, K. Tanaka and Y. Tamura, "Field measurement of damping and natural frequency of an actual steel-framed building over a wide range of amplitudes", *Journal of wind engineering and industrial aerodynamics*, vol. 59, no. 2-3, pp. 325–347, 1996. DOI: 10.1016/0167-6105(96)00015-3.
[42] "Acoustics - determination of sound power levels and sound energy levels of noise sources using sound pressure - engineering methods for an essentially free field over a reflecting plane", International Standard, Case Postale 56, Standard, Oct. 2010.
[43] "Buller", Arbetsmiljöverkets författarsamling, 171 84 Solna, Standard, Mar. 2005.
[44] Ansys. (n.d.). Absorbing boundary condition (abc), [Online]. Available: https://ansyshelp.ansys.com/account/secured?returnurl=/Views/Secured/corp/v201/en/ans_acous/acous_bc_abc.html (visited on 06/05/2020).
[45] ——, (n.d.). Surface impedance boundary, [Online]. Available: https://ansyshelp.ansys.com/account/secured?returnurl=/Views/Secured/corp/v201/en/ans_acous/acous_bc_apply.html%5C%23acous_bc_surfimp (visited on 06/05/2020).
[46] ——, (n.d.). Artificially matched layers, [Online]. Available: https://ansyshelp.ansys.com/account/secured?returnurl=/Views/Secured/corp/v201/en/ans_acous/acous_artificial.html (visited on 06/05/2020).
[47] ——, (n.d.). Elements for acoustic analysis, [Online]. Available: https://www.mm.bme.hu/~gyebro/files/ans_help_v182/ans_elem/elem_acouselems.html (visited on 06/05/2020).

Appendix

A Engine Loads

In Table 6.1 and 6.2 the values of the free mass loads from engine order one to three can be seen at four discrete speeds ranging between 1,250 to 2,000 rpm. The forces F_x and F_z are in the plane normal to the crankshaft while the torque T_x is about the crankshaft, seen in Figure 1.5.

Table 6.1: *Values of the free mass loads at the speeds 1,250 and 1,500 rpm of the Stirling engine.*

Order	Load	1,250 rpm Magnitude [Nm or N]	1,250 rpm Phase [rad]	1,500 rpm Magnitude [Nm or N]	1,500 rpm Phase [rad]
1	F_x	132.47	0.58	190.36	0.59
	F_z	138.47	1.63	200.67	1.62
	T_y	1.02	-0.46	1.51	-0.44
2	F_x	232.49	0.67	334.78	0.67
	F_z	155.09	2.38	223.31	2.38
	T_y	4.51	1.10	6.51	1.10
3	F_x	16.08	2.10	23.14	2.10
	F_z	5.79	-2.19	8.35	-2.19
	T_y	4.27	1.83	6.16	1.83

Table 6.2: *Values of the free mass loads at the speeds 1,750 and 2,000 rpm of the Stirling engine.*

Order	Load	1,750 rpm Magnitude [Nm or N]	1,750 rpm Phase [rad]	2,000 rpm Magnitude [Nm or N]	2,000 rpm Phase [rad]
1	F_x	258.77	0.59	338.20	0.59
	F_z	274.18	1.62	358.23	1.62
	T_y	2.09	-0.44	2.76	-0.43
2	F_x	455.71	0.67	595.17	0.67
	F_z	303.96	2.38	396.97	2.38
	T_y	8.86	1.10	11.58	1.10
3	F_x	31.49	2.10	41.10	2.10
	F_z	11.36	-2.19	14.84	-2.19
	T_y	8.38	1.82	10.94	1.83